OPTIMIZATION OF ONSHORE STEEL DRILLING RIGS USING THE
CONVERGENCE RATE APPROACH INTEGRATED METAHEURISTIC
SEARCH ALGORITHMS

A THESIS SUBMITTED TO
THE GRADUATE SCHOOL OF NATURAL AND APPLIED SCIENCES
OF
MIDDLE EAST TECHNICAL UNIVERSITY

BY

REZA SALATIN

IN PARTIAL FULFILLMENT OF THE REQUIREMENTS
FOR
THE DEGREE OF MASTER OF SCIENCE
IN
CIVIL ENGINEERING

JULY 2018

Approval of the thesis:

OPTIMIZATION OF ONSHORE STEEL DRILLING RIGS USING THE CONVERGENCE RATE APPROACH INTEGRATED METAHEURISTIC SEARCH ALGORITHMS

submitted by **REZA SALATIN** in partial fulfillment of the requirements for the degree of **Master of Science in Civil Engineering Department, Middle East Technical University** by,

Prof. Dr. Halil Kalıpçılar
Dean, Graduate School of **Natural and Applied Sciences**   _____

Prof. Dr. İsmail Özgür Yaman
Head of Department, **Civil Engineering**   _____

Prof. Dr. Oğuzhan Hasançebi
Supervisor, **Civil Engineering Dept., METU**   _____

Assist. Prof. Dr. Halit Cenan Mertol
Co-Supervisor, **Civil Engineering Dept., Atilim University**   _____

Examining Committee Members:

Assist. Prof. Dr. Onur Pekcan
Civil Engineering Dept., METU   _____

Prof. Dr. Oğuzhan Hasançebi
Civil Engineering Dept., METU   _____

Assist. Prof. Dr. Saeid Kazemzadeh Azad
Civil Engineering Dept., Atilim University   _____

Assoc. Prof. Dr. Eray Baran
Civil Engineering Dept., METU   _____

Assist. Prof. Dr. Halit Cenan Mertol
Civil Engineering Dept., Atilim University   _____

Date: July 30, 2018

I hereby declare that all information in this document has been obtained and presented in accordance with academic rules and ethical conduct. I also declare that, as required by these rules and conduct, I have fully cited and referenced all material and results that are not original to this work.

Name, Last Name: Reza Salatin

Signature:

ABSTRACT

OPTIMIZATION OF ONSHORE STEEL DRILLING RIGS USING THE CONVERGENCE RATE APPROACH INTEGRATED METAHEURISTIC SEARCH ALGORITHMS

Salatin, Reza
M.Sc., Department of Civil Engineering
Supervisor: Prof. Dr. Oğuzhan Hasançebi
Co-Supervisor: Assist. Prof. Dr. Halit Cenan Mertol

July 2018, 112 pages

Despite the exceptional ability of the metaheuristics in locating the optimum solution of discrete optimization problems, the volume of the required analyses through these methods is burdensome. Optimization of large-scale structures having numerous load cases, as well as complex geometries, therefore, is not considered practical in construction industry. In current study, however, an effort has been made to pave the way for the industrialization of the structural optimization by enabling the traditional metaheuristics to efficiently solve the large-scale structural problems. Therefore, the so-called Convergence Rate approach is hybridized into two well-established optimization methods to reduce the computational effort of the metaheuristics.

Initially, the newly proposed approach, which is named the Convergence Rate method, is developed and integrated into the Adaptive Dimensional Search and Exponential Big Bang-Big Crunch optimization methods. Through this method, not only have non-improving candidates been deleted from the optimization process, but the rest of the candidates within a population also have been excluded from the analyses once an improved solution within the expected range is unearthed from the same population.

Thereafter, the proposed algorithm is tested on a large-scale onshore drilling rig structure having various load cases as well as a complex geometry. In the end, nonetheless the elimination of the vast majority of the candidate solutions from the analyses, the algorithm demonstrates a promising performance in locating the optimum solution of the problems.

ÖZ

SEZGİ ÜSTÜ ALGORİTMALARA ENTEGRE OLMUŞ YAKINSAMA ORANI YAKLAŞIMI İLE KARADA OLAN ÇELİK SONDAJ KULELERİNİN OPTİMİZASYONU

Salatin, Reza
Yüksek Lisans, İnşaat Mühendisliği Bölümü
Tez Yöneticisi: Prof. Dr. Oğuzhan Hasançebi
Ortak Tez Yöneticisi: Dr. Öğr. Üyesi Halit Cenan Mertol

Temmuz 2018, 112 sayfa

Optimizasyon problemlerinde optimum noktanın yerini belirlemede sezgi üstü algoritmaların olağanüstü yeteneklerine rağmen, bu yöntemlerle gerekli analizlerin hacmi fazladır. Bu nedenle, çok sayıda yük ve karmaşık geometrilere sahip büyük ölçekli yapıların optimizasyonu inşaat sektöründe pratik olarak kabul edilmemektedir. Mevcut çalışmada, geleneksel sezgi üstü algoritmaların büyük ölçekli yapısal problemleri etkin bir şekilde çözebilmelerini sağlayarak yapısal optimizasyonun sanayileşmesinin önünü açmak için çaba gösterilmiştir. Bu nedenle, Yakınsama Oranı yaklaşımı, sezgi üstü algoritmaların hesaplama çabasını azaltmak için iki optimizasyon yöntemine hibridize edilimiştir.

İlk olarak, Yakınsama Oranı yaklaşımı, Adaptive Dimensional Search ve Exponential Big Bang-Big Crunch optimizasyon yöntemlerine entegre edilerek geliştirilmiştir. Bu yöntemle, iyileştirici olmayan adaylar sadece optimizasyon sürecinden çıkarılmış olmakla kalmayıp, aynı popülasyondan beklenen aralık içinde geliştirilmiş bir çözüm ortaya çıkarıldığında, bir popülasyon içindeki adayların geri kalanı da analizlerden çıkarılmıştır.

Daha sonra, önerilen algoritma, çeşitli yük durumları ve karmaşık bir geometriye sahip büyük ölçekli bir kıyı sondaj kulesi üzerinde test edilimiştir. Sonuçta, yine de aday çözümlerinin büyük çoğunluğunun analizlerden çıkarılması, algoritmanın problemlerin optimum çözümünü bulmada ümit verici bir performans sergilediğini göstermektedir.

Anahtar Kelimeler: Yapısal Optimizasyon, Çelik Tasarım, Boyutlandırma Optimizasyonu, Çelik Çerçeveler, Çelik Makaslar

To My Family

ACKNOWLEDGMENTS

TABLE OF CONTENTS

LIST OF TABLES

LIST OF FIGURES

FIGURES

xvi

LIST OF ABBREVIATIONS

ABBREVIATIONS

ADS	Adaptive Dimensional Search
BB	Big Bang-Big Crunch
CR	Convergence Rate
CRC	Convergence Rate Coefficient
EBB	Exponential Big Bang-Big Crunch
GADS	Guided Adaptive Dimensional Search
GADS-EBB	Guided Adaptive Dimensional Search-Exponential Big Bang-Big Crunch
GEBB	Guided Exponential Big Bang-Big Crunch
GSS	Guided Stochastic Search
MBB	Modified Big Bang-Big Crunch
PSO	Particle Swarm Optimization
RMF	Rate Modification Factor
SEP	Stagnation Escape Period
TE	Travelling Equipment
UB	Upper Bound

CHAPTER 1

INTRODUCTION

1.1. Structural Optimization

Rather than being a pure mathematical method, optimization tends to be an intrinsic part of entities. Organisms have developed special physical and cognitive characteristics to adapt their bodies with the most severe environments. The same procedure applies to the engineering applications, as well. Construction costs have always been a disadvantage in engineering design and have urged structural engineers to lower the weight of the structures to the least possible values, as long as the limitations of robustness and serviceability are not violated.

Every structural optimization problem is composed of three chief components. Input data, which are known as the (i) Design Variables, are analyzed through a procedure named as the (ii) Objective Function of the optimization problem. A broad range of criteria, which are referred to as the (iii) Design Constraints, define the boundaries imposed upon the selection of the design variables. Through this procedure, thus, a set of parameters $\{I_n\}$ are obtained that minimize the objective function $f(I_0, \dots, I_n)$ of the problem.

Optimization methods can be classified as either traditional or modern techniques. Conventional optimization methods including the mathematical programming (Adeli & Kamal, 1986; Erbatur & Al-Hussainy, 1992; Hager & Balling, 1988) and optimality criteria (Saka, 1991; Venkayya, 1978) search for a local optimum point by moving in a path led by the local gradient information. These methods, therefore, are inefficient in dealing with problems having numerous and discrete design variables (Belegundu & Arora, 1985). Furthermore, since these methods search for

a solution in the vicinity of the initial point, if there are a plenty of local optimum solutions within the search space, outcomes will depend on the starting point. Thus, the algorithm will most likely fail to locate the global optimum point and will consequently be trapped in a local optimum solution (Lee & Geem, 2004).

However, modern optimization techniques, which have gained popularity in recent years and compose a significant part of the state of the art global optimization methods (Yang 2013), do not require initial values and substantial gradient information, and use a random search method, instead (Lee & Geem, 2004).

Optimization can be carried out on the size, topology, and shape of the structures. Size optimization is performed through modification of the structural cross sections to acquire the minimum value of the structure's weight. Structural cross sections, which are the variables of the problem, can have continuous or discrete form. In continuous size optimization, the cross-sectional values may take any positive real number, while in the discrete form, which is more applicable to the real-world structural problems, the cross sections should be selected from a standard list containing the available sections in the market. Likewise, topology optimization, is implemented through the addition and removal of the structural nodes and elements of a structure, while shape optimization is accomplished through shifting the nodes. These two optimization categories, though can simultaneously be performed with the size optimization (Ahrari et al, 2015; Tejani et al, 2018), are out of the scope of this thesis.

1.2. Metaheuristic Optimization Algorithms

Back in 1948, Alan Turing published his innovative ideas in machine learning, neural networks, and evolutionary algorithms. Later in 1960s and 1970s, John Holland developed Genetic Algorithm which was inspired by Darwin's theory on natural selection. This method utilized the natural selection theory ideas including crossover, mutation, fitting, and selecting the fittest (Holland, 1992); moreover, it represented the solutions in a genetic form, generated a random initial population of solutions, evaluated each solution, rated them according to their fitness, and

employed the crossover operator to modify the genetic composition of individuals in a population for the generation of population for the next iteration of analyses (Kameshki & Saka, 2001). This method paved the way for the emergence of numerous evolutionary algorithms named as 'Metaheuristics'.

Metaheuristics means 'proceeding to a solution by trial and error'. Metaheuristics are appropriate for locating the global optimum since in addition to exploiting (local search) the design space, they are also capable of exploring (random global search) it (Yang 2010).

Some of the most prominent metaheuristic optimization methods include Particle Swarm (Kennedy & Eberhart 1995), Ant Colony (Dorigo & Stützle, 2004), and Artificial Bee Colony (Karaboga & Basturk, 2007) optimization techniques. Numerous studies have been carried out on these methods to improve their performance through modification of their basic parameters such as step size (Nickabadi et al, 2011; Shi & Eberhart 2001) or through hybridization with other optimization algorithms (Kaveh & Talatahari, 2009a). Notwithstanding their various names and inspiration sources, most of the metaheuristic algorithms share similar formulation (Hasançebi & Azad, 2015).

Metaheuristics search the design space iteratively in order to locate the optimum solution of the problem. However, there is always a possibility that the algorithm will be trapped in a local optimum or the algorithm will meet the termination criterion, which is mostly the maximum number of iterations, before it reaches the optimum solution.

1.3. Aim and Scope of the Thesis

In this study, two main objectives are sought: initially a new strategy for reducing the computational effort and increasing the efficiency of the metaheuristic search algorithms is proposed and is integrated into two well-established optimization methods namely the Adaptive Dimensional Search (ADS) and Exponential Big Bang-Big Crunch (EBB) algorithms; secondly, the new code is employed for

optimum design of an onshore drilling rig structure considering the relevant professional standards. Since the various loading conditions and complex geometries of the large-scale structures have been considered as the drawbacks of the metaheuristic algorithms, employing a computationally efficient and robust optimization method is crucial for a fast converging, yet precise, solution.

Chapter 2 of the thesis is devoted to the design problem formulation of the onshore drilling rigs through the relevant standards and local conditions. Mathematical formulization of the size optimization of steel trusses and frames using the ASD-AISC (1989) specification is outlined in Chapter 3. Meanwhile, Chapter 4 is dedicated to the formulation of the proposed Convergence Rate approach, Adaptive Dimensional Search method, Exponential Big Bang-Big Crunch method, Upper Bound approach, and Stagnation Control strategy. Later in this chapter, the Upper Bound strategy, as well as the Convergence Rate strategies are integrated into the ADS and EBB metaheuristic algorithms and the results of three benchmark problems optimized with these methods are compared within the consecutive chapter. Chapter 6, though, is committed to the optimum design of an onshore drilling rig structure through the newly proposed Convergence Rate approach integrated Adaptive Dimensional Search and Exponential Big Bang-Big Crunch methods. Finally, Chapter 7 is specified for concluding remarks of the thesis and some of its important outcomes. In the end, a few recommendations for further studies are provided.

CHAPTER 2

DESIGN PROBLEM FORMULATION OF ONSHORE DRILLING RIGS

2.1. Introduction

Drilling rigs are utilized for drilling multi-purpose wells in the earth's surface. These rigs are categorized either as offshore or onshore structures and can be in various sizes and shapes as illustrated in Figure 2.1. While smaller rigs with a limited drilling capacity can be mounted on trucks and trailers, large offshore drilling units can drill the earth's surface for thousands of meters and can provide housing for tens of people. These improvements in their function and structure, however, have been obtained through the last two centuries.

2.2. Onshore Drilling Rigs

Invention of the first four-legged derricks dates back to 1825. The main columns of the derrick consisted of the square timber woods and were designed in a flexible and easy to dismantle way. Later in 1859, Bissell and Drake successfully drilled a 21 m commercial well using a wooden drilling rig. Indeed, Drake was the first American to invent the oil wells. His rig, however, had two serious weaknesses. First, the rig could not be dismantled and set up in a new drilling location and thus, after the drilling was finished, the rig would be left at the drilling site permanently. Second, since the rig was made of wood, it could not be utilized for drilling deeper wells and thus, its usage was limited to the shallow wells. Both of the wooden rigs are illustrated in Figure 2.2. The advent of the steel derricks, though, dates back to 1912 when Moore (2018) patented a system of securely clamping the braces to the steel pipes, and thus, constructed the first steel derrick. The efficiency of the system

led to the mass substitution of the wooden derricks by the newly invented steel derricks till 1930.
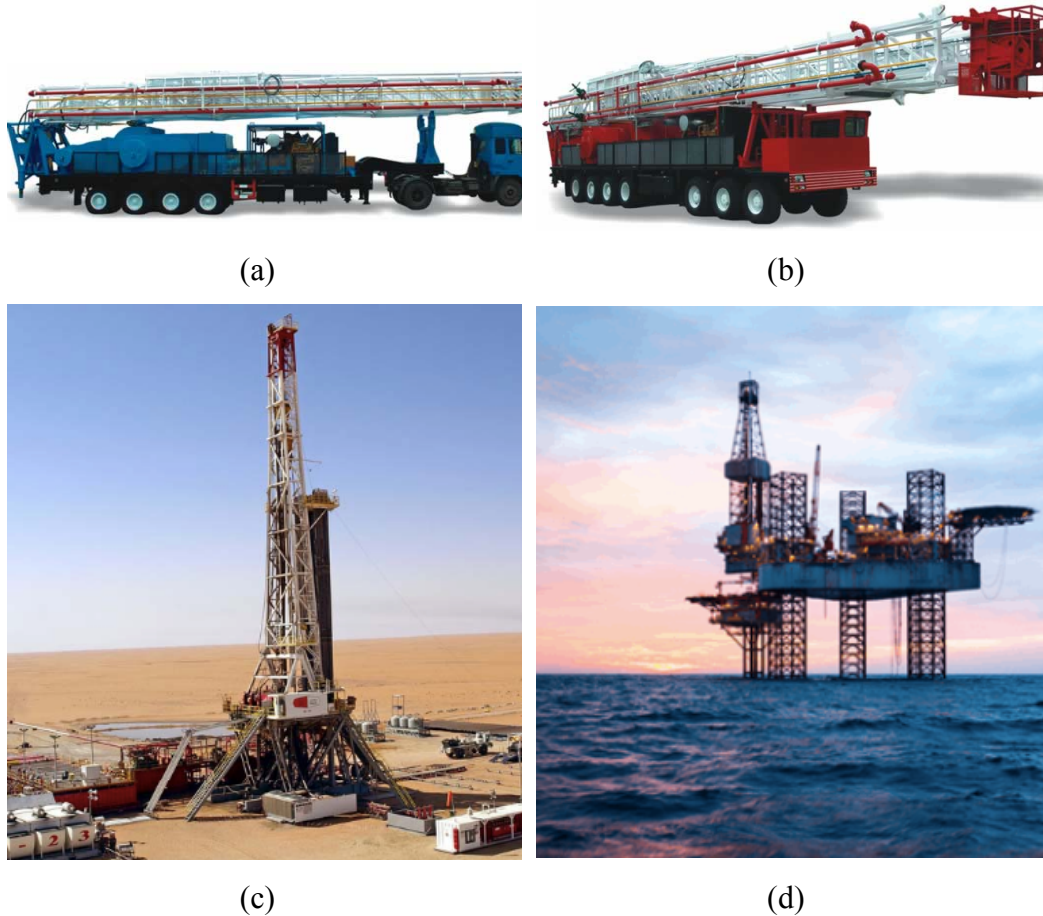
Figure 2.1. Modern Drilling Rig Types

(a) Trailer Mounted Drilling Rig (Sunnda Corporation, 2018); (b) Truck Mounted Drilling Rig (Sunnda Corporation, 2018); (c) Onshore Skid Mounted Drilling Rig (Arabian Drilling Company, 2018); (d) Offshore Jack-up Drilling Rig (Rigzone Inc., 2018)

The improvements on the structure of the drilling rigs, however, is still in progress and with the advent of the modern onshore drilling rigs, as illustrated in Figure 2.1(c), not only can drillings be made for depths more than 6000 meters, but also it can be carried out in a much less time compared to the old rigs. Moreover, the modern rigs are also designed for different environmental conditions, such as deserts and cold regions.

(a)   (b)
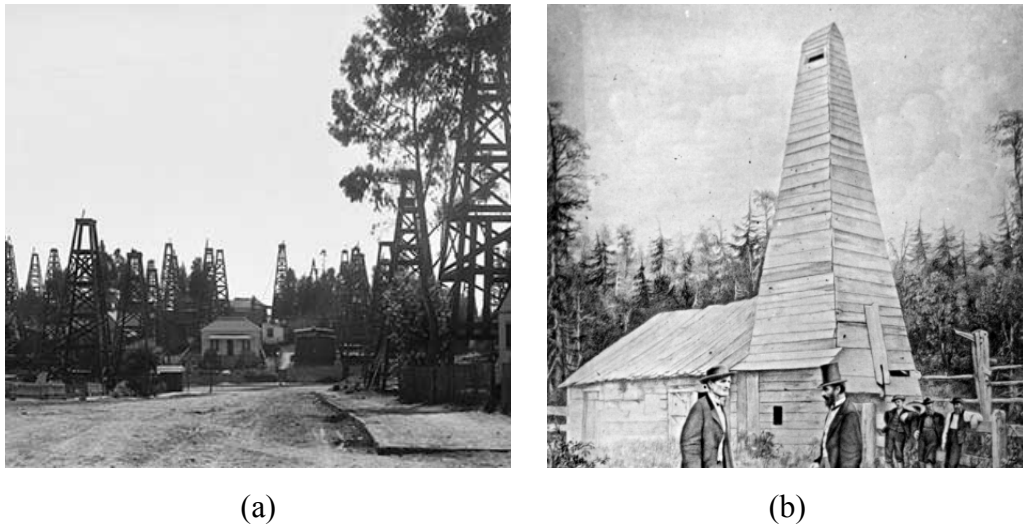
Figure 2.2. Conventional Drilling Rigs Types
(a) First Four-Legged Derrick, 1825 (b) Drake Drilling Rig, 1859 (National Driller Magazine, 2018)

Drilling rigs are composed of four main systems including the hoisting, power generation, mud circulation, and well control systems. While the initial system is a matter of interest within this study, the latter systems are out of the scope of this

thesis and will not be addressed. Hoisting system is composed of the following units:

- Mast
- Substructure
- Crown Assembly and Travelling Equipment (TE)
- Top Drive
- Rotary Table

The explanation of which are provided within the following sections.

2.2.1. Mast

As depicted in Figure 2.3, masts are structural latticed towers of rectangular cross section with an open face (API Specification 4F, 2013). These towers are generally composed of one or more separate parts which are connected to each other in a horizontal position and then, the mounted tower is erected to a vertical position using hydraulic jacks. Masts are mostly employed in onshore drilling rigs, while derricks are utilized in offshore drilling units and refer to steel towers with different geometries. Furthermore, masts have some advantages over derricks including one open side, which allows the travelling equipment to move freely along the height of the tower.

2.2.2. Substructure

As illustrated in Figure 2.4, substructure is a platform under the mast tower which is used for supporting the mast, drill pipes, oil well dog house, driller's cabin, and many other smaller drilling equipment. Moreover, it provides a working area referred to as Drill Floor for the personnel, as well.

2.2.3. Crown Assembly and Traveling Equipment

Crown assembly and travelling equipment, together with the wire ropes, comprise a system for lifting the weight of the hook load. While crown assembly is a group

of sheaves fixed at the top of the mast, its companion group of blocks, which are referred to as the traveling equipment, can freely move in a distance between the crown block and the rig floor. Figure 2.5 illustrates the hoisting system composed of the crown block, travelling equipment, and the wire ropes.

Figure 2.3. Mast (Loadmaster Universal Rigs Inc., 2018)

2.2.4. Top Drive

Top drive is a mechanical device in modern drilling rigs that provides a torque to the drilling pipes to drill a borehole. This device has succeeded the rotary table in past drilling units which was able to drill 9.1 m in one operation. The top drive system, however, is able to drill 27.3 m in one operation making it an efficient and time saving method in drilling boreholes. The stability of the top drive is guaranteed by the guide beam which is located behind the top drive and transfers the torque produced by the top drive to the mast structure.

Figure 2.4. Substructure (GlobalSpec, 2018)

2.2.5. Rotary Table

Rotary Table is a mechanical device in drilling rigs that is used to provide a torque to the drilling pipes to drill a borehole. This device has been succeeded by the top drive in modern drilling rigs. The slip at the center of the rotary table, however, is

utilized for holding the drill string for connecting the new pipes to the drill string as illustrated in Figure 2.6.

2.2.6. Driller's Cabin

Driller's Cabin is located on the substructure and is cantilevered out from the drilling floor. This cabin not only offers a safe and temperature-controlled place for the rig personnel in harsh environments, but also includes an interface for controlling every tool located on the rig.

2.2.7. Oil Well Dog House

Oil Well Dog House is located on the substructure and similar to the driller's cabin is cantilevered out from the drilling floor. This cabin, however, is utilized for general meeting purposes and does not include any specific drilling facilities.
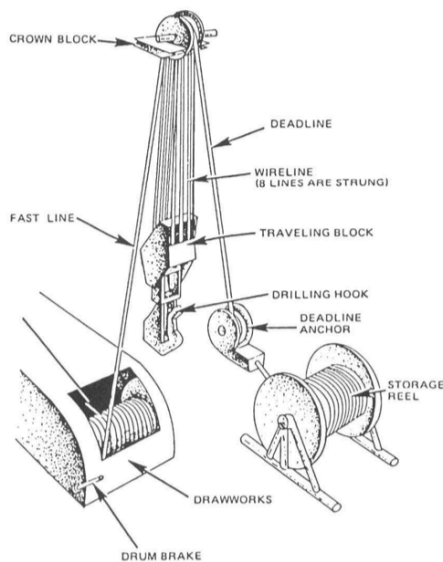
Figure 2.5. Hoisting System (Sampayo 2007)

2.2.8. Racking Board

As illustrated in Figure 2.7, Racking Board is a device on the mast mainly employed as a support for drilling pipes. While each drilling pipe is as long as 9.1 m, they are screwed to each other to make a single pipe of 27 m in length and then are stored on the setback area for future use. While the substructure plays a crucial role in supporting the weight of the drilling pipes, which is referred to as setback load, these pipes are stabilized at the other end through the racking board.
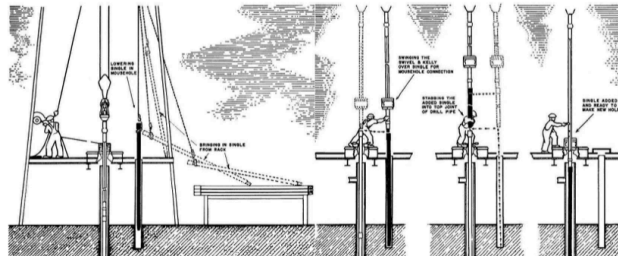
(a)
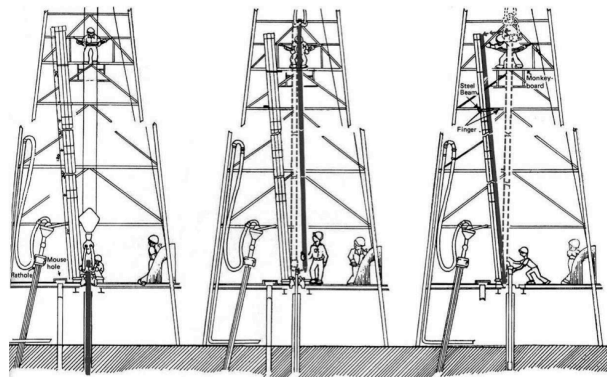
(b)

Figure 2.6. (a) adding and (b) Removing the drilling pipes (Sampayo 2007)

2.3. Structural Modeling

A detailed modeling and design procedure of the onshore steel drilling rig structures is outlined in the following sections.
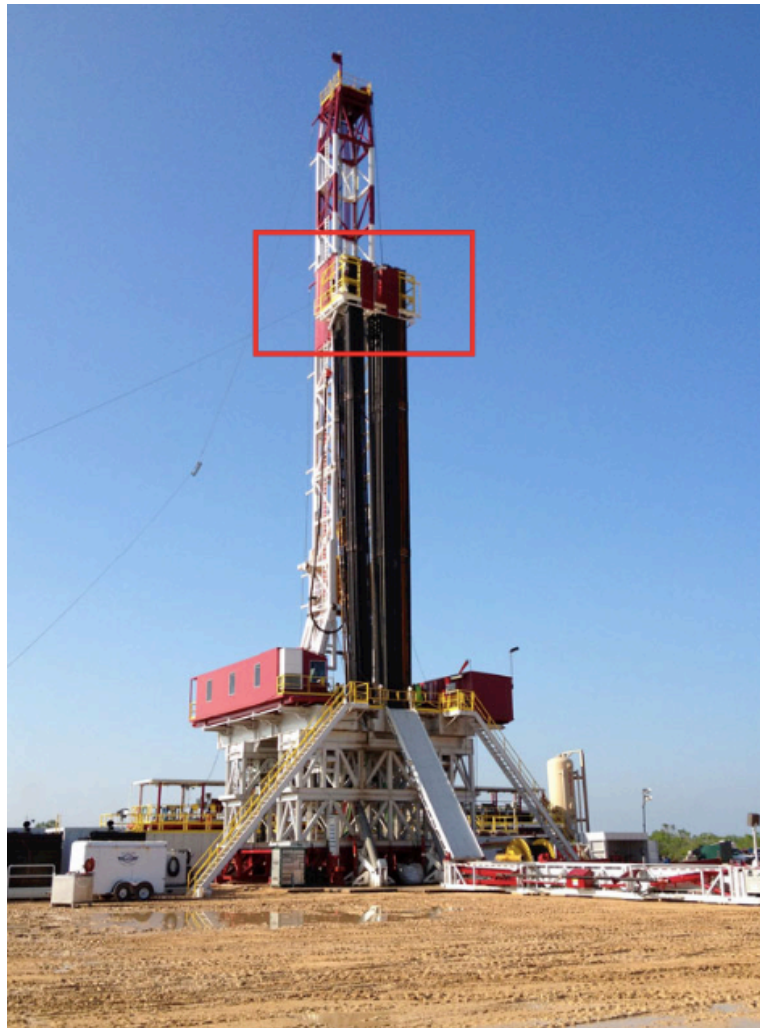
Figure 2.7: Racking Board (Drilling Contractor, 2018)

2.3.1. Structural Layout

An analytical model of a land rig is generated in SAP2000 v19.2.2 (2017) software. The geometrical information of the structure is illustrated in Figure 2.8. Mast and substructure of the drilling rig are modeled for analysis and design purposes. Drilling pipes and cabins, however, are modeled solely for absorbing the wind loads imposed upon the structure without having a structural role. Heights of the substructure and mast are 7.6 and 44.2 m, respectively, comprising a total height of 51.8 m for the rig.

| (a) | (b) | (c) |
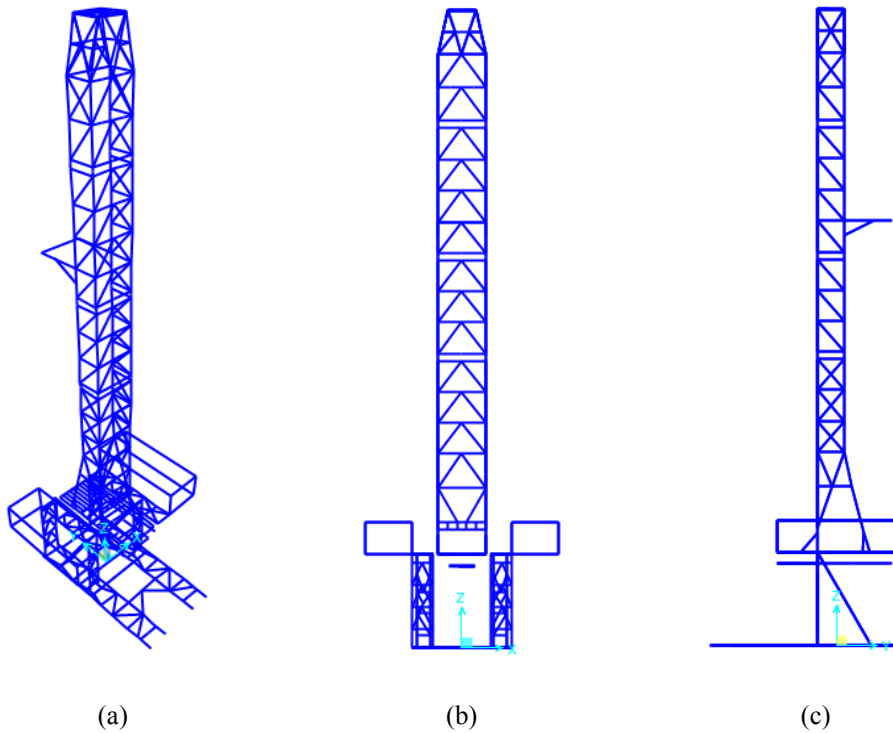
Figure 2.8. Layout of a Land Rig (a) 3-D View, (b) Front View, (c) Side View

The mast can be divided into four separate parts, including the Top, Mid-top, Mid-low, and Lower parts as represented in Figure 2.9. This feature reduces the length of the structural parts for transportation purposes and thus conforms to the local transportation rules.

(a)   (b)   (c)   (d)
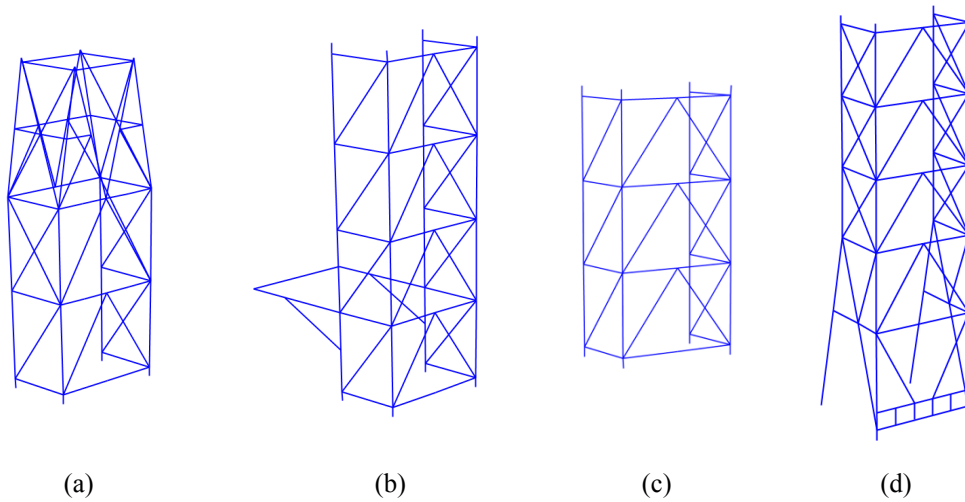
Figure 2.9. 3-D Views of the Mast Parts

(a) Top (b) Mid-Top (c) Mid-Low (d) Lower

The substructure is also constructed of several parts. The substructure surface which is located at the height of 7.6 meters is used as the drilling floor; the eight columns of the substructure transfer the loads to the ground; and the structural elements at the ground level provide the structure with the required stability either in erection or in in-place stages.
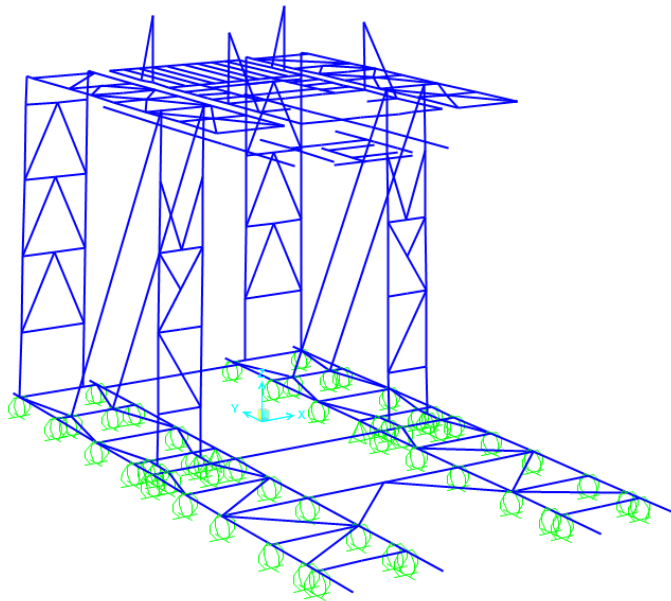
Figure 2.10. 3-D View of the Substructure Part

2.3.2. Design Bases

Drilling rigs are designed according to the API 4F (2013) standard. While this standard is the main reference which should be considered in all design practices, it refers to other standards relevant to the specific parts of the design process. The standards employed for each design part are outlined as follows:

- API Specification 4F (2013), Specification for Drilling and Well Servicing Structures

- AISC-ASD (1989), Specification for Structural Steel Buildings, Allowable Stress Design

- API RP 2A-WSD (2014), Recommended Practice for Planning, Designing and Constructing Fixed Offshore Platforms-Working Stress Design

- ASCE/SEI 7-05 (2006), Minimum Design Loads for Buildings and Other Structures

- Turkish Seismic Code 2007

2.3.3. Local Conditions

A summary of local environmental conditions selected for the drilling rig is illustrated in Table 2.1.

Table 2.1: local conditions

Maximum Temperature	+50 °C
Minimum Temperature	-30 °C
Reference Wind Velocity - Operational	40 knots
Reference Wind Velocity - Unexpected	70 knots
Reference Wind Velocity - Expected	95 knots
Seismic Zone	Zone 1
Site Class	Z3
Building Importance Factor	1.2

2.3.4. Structural Safety Level

Structural Safety Level is related to the various degrees of consequence of a failure including life safety, pollution, economic loss, and public concern. Referring to the API 4F (2013) standard, the appropriate SSL for a drilling rig structure should be selected according to the Table 2.2. A medium importance factors for life safety, pollution, economic loss, and public concern which are denoted by the E2 or U2

have been selected within the current study. This level of structural safety is for the structures with medium consequences of failure. This factor is utilized when determining the building importance factor as well as the structural safety level multiplier which will be discussed within the following sections.

Table 2.2: Structural Safety Level

Life Safety	Pollution, Economic Loss, Public Concern, etc.		
	High	Medium	Low
High	E1 or U1	E1 or U1	E1 or U1
Medium	E1 or U1	E2 or U2	E2 or U2
Low	E1 or U1	E2 or U2	E3 or U3

2.3.5. Load Combinations

According to the API 4F (2013) standard, all drilling structures shall be designed based on the load combinations illustrated in Table 2.3, where the load combinations are provided through the participation percentages of the load cases. Five major load cases compose the design load combinations. Dead Load is the weight of the structural elements as well as the weight of the equipment attached to the structure. A detailed explanation of the equipment load is provided in the following sections. Hook load is either the weight of the drill string or travelling equipment (TE); rotary load is the weight of the drill string supported by the rotary table; setback load is the weight of the drilling pipes stored on the setback area; and environmental loads denote either the wind or seismic loads.

2.3.6. Main Loads

Main loads imposed upon the drilling rig structure according to the API 4F (2013) standard are outlined below.

2.3.6.1.   Dead Load

Dead load is the weight of the structural steel elements comprising the structure. Type of the steel material being utilized is ASTM A514 (B) alloy steel which is used for structural applications requiring high strength steel material. Mechanical properties of the ASTM A514 (B) alloy steel are illustrated in Table 2.4.

2.3.6.2.   Maximum Rated Static Hook Load

According to the API 4F (2013) standard, maximum rated static hook load is the weight of the travelling equipment and a static load applied to the travelling equipment. Hook Load is the total weight of the drilling pipes pulling down on the hook. This load capacity is an important factor in determining the drilling rig type. In addition to a downward load, there are also fast line and dead line loads comprising the hook load of the drilling structure. The hook load is carried by a set of ropes as denoted in Figure 2.11, where W denotes the wieght of the drill string as well as the travelling equipment. Moreover, F_f and F_s denote the fast line and dead line loads, respectively. Likewise, F_d denotes the load imposed upon each of the columns.

Fast line is part of the rope connecting the crown block to the draw-works, whereas, deadline is a part connecting the crown block to an anchor point. Fast line and dead line loads can be calculated according to the hook load capacity of the structure, as well as the number of lines hanging from the crown block. It should be mentioned that for the system being studied, a 12-line hoisting system carries the hook load.

Table 2.3: Load Combinations for Drilling Structures

Load Case	Loading Condition	Dead Load	Hook Load	Rotary Load	Setback Load	Environmental Loads
1a	Operating	100	100	0	100	Operating Wind
1b	Operating	100	TE*	100	100	Operating Wind
2	Expected	100	TE	100	0	Expected Storm
3a	Unexpected	100	TE	100	100	Unexpected Storm
3b	Unexpected	100	AA**	AA	AA	Earthquake
4	Erection	100	AA	AA	0	Erection Wind
5	Transportation	100	AA	AA	AA	Transportation Wind

* Travelling Equipment
** As Applicable

Table 2.4: Mechanical Properties of the ASTM A514 (B) Alloy Steel

Mechanical Property	Value
Minimum Yield Stress, F_y	690 MPa
Minimum Tensile Stress, F_u	760 MPa
Modulus of Elasticity, E	210000 MPa
Shear Modulus, G	80000 MPa
Density	7.85 gr/cm^3
Poisson's Ratio, ν	0.3
Thermal Expansion Coefficient, α	1.170E-05
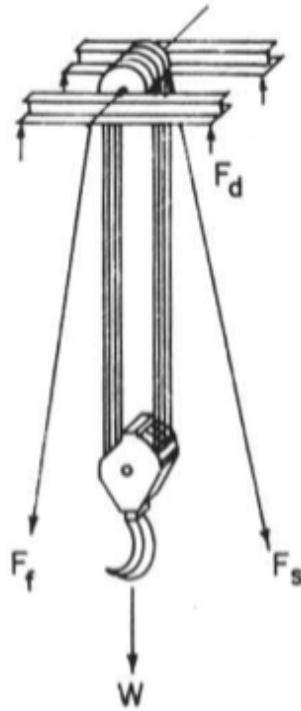
Figure 2.11. Hoisting System Carrying the Hook Load (Sampayo 2007)
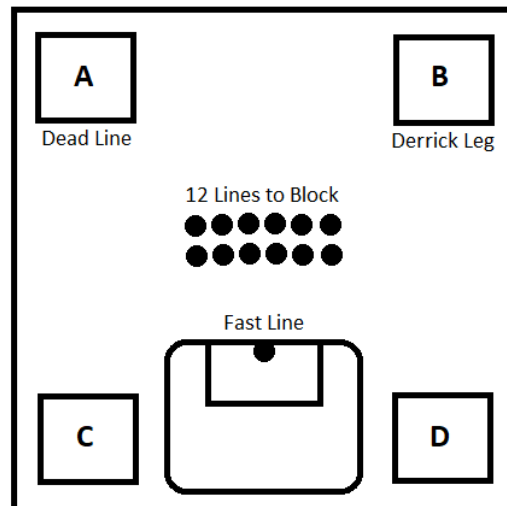
Figure 2.12. Mast floor plan (Sampayo 2007)

According to the API RP 9B (2005), the fast line efficiency and fast line factor for a travelling block with 12 ropes supporting the hook load are as follows:

$$Efficiency\ (E) = 0.782$$
$$Number\ of\ lines\ (N) = 12$$

Thus, the value of fast line and dead line loads can be calculated according to the Eqs. (2.1) and (2.2), respectively (API Recommended Practice 9B, 2005).

$$Fast\ Line\ Load = \frac{Hook\ Load}{N \times E} \tag{2.1}$$

$$Dead\ Line\ Load = \frac{Hook\ Load}{N} \tag{2.2}$$

Therefore, the hook load values exerted upon four columns of the mast can be calculated as follows:

$$F_A = \frac{Hook\ Load}{4} + Dead\ Line\ Load = 116.67\ tonf$$

$$F_B = \frac{Hook\ Load}{4} = 87.50\ tonf$$

$$F_C, F_D = \frac{Hook\ Load}{4} + Fast\ Line\ Load = 124.80\ tonf$$

$$F_{total} = F_A + F_B + F_C + F_D = 453.77\ tonf$$

In addition to the aforementioned load, a top drive torque of $760.40\ tonf.cm$ is also exerted upon the guide beam.

2.3.6.3.   Rated Static Rotary Load

According to the API 4F (2013), rated static rotary load is the maximum weight that can be supported by the rotary table support beams. Since the rig being designed falls within the category of modern rigs using the top drive system, rotary table is only used for supporting the vertical hook load while adding extra pipes to the drill string. Therefore, no torque is exerted upon the rotary table support beams,

and a sole rotary load of 350 $tonf$ is applied upon the rotary table as a distributed area load.

Table 2.5: Rotary Load

Load Case	Distributed Vertical Load (tonf/m²)	Moment (tonf-m)	Load Factor	Impact Factor	Total Vertical Load (tonf)
Rotary Load	111.1	0	1.0	1.0	350

2.3.6.4.   Rated Setback Load

According to the API 4F (2013), rated setback load is the maximum weight of tubular goods that can be supported by the substructure in the setback area. A setback load of 250 $tonf$ is exerted upon the setback beams as a distributed frame load.

Table 2.6: Setback Load

Load Case	Distributed Vertical Load (tonf/m)	Moment (tonf-m)	Load Factor	Impact Factor	Total Vertical Load (tonf)
Setback Load	10.0	0	1.0	1.0	250

2.3.6.5. Equipment Load

Weight of the equipment attached to the drill rig, as well as their working moment is illustrated in Table 2.7. Based on the Section 4.7 of the ASCE 7 (2006), an impact factor is also applied on the equipment weights to allow for ordinary impact conditions in applications containing unusual vibration and impact forces. According to the abovementioned standard, while for the (i) light machinery and shaft/motor driven units the factor is equal to 1.2, for the (ii) reciprocating machinery and power-driven units the factor is equal to 1.5. Furthermore, in order to cover the uncertainties in the value of the equipment weights, all machinery weights are also increased by 20%.

2.3.6.6. Wind Load

Application of the wind load on the rig structure should conform to the Section 8.3 of the API 4F (2013). According to this standard, the following wind environments should be considered when analyzing the structure.

- **Operational Condition:** Within this environmental condition, unrestricted drilling operations may be carried out.

- **Unexpected Storm Wind:** Unexpected storm refers to a sudden hurricane or storm, where there is a shortage of time for preparations and setback lowering. Therefore, setback should be considered in wind load computations.

- **Expected Storm Wind:** Expected storm refers to a known hurricane or storm, where there is ample time for preparations and setback lowering.

- **Erection Wind:** Erection condition refers to the wind condition under which rig erection operations may be carried out.

- **Transportation Wind:** Transportation condition refers to the wind condition under which special transportation operations may be continued.

Table 2.7: Equipment Load

Load Case	Vertical Load (tonf)	Moment (tonf-m)	Load Factor	Impact Factor
Guide Beam	10.0	7.6	1.2	1.0
Travelling Block	11.0	-	1.2	1.0
Iron Roughneck	4.5	9.3	1.2	1.5
Power Slip	2.5	-	1.2	1.0
Rotary Table	9.0	-	1.2	1.5
Oil Well Dog House	8.5	14.0	1.2	1.0
Drillers Cabin	9.0	15.5	1.2	1.0
Top Drive	26.5	-	1.2	1.2
Crown Assembly	10.0	-	1.2	1.2
Racking Board	5.0	-	1.2	1.0
Ladder and Rest Platforms	1.5	-	1.2	1.0
Climb Assist Device	0.3	-	1.2	1.0
Racking Board Escape Device	0.2	-	1.2	1.0
Lights and Cables	1.1	-	1.2	1.0
Air and Hydraulic Piping	1.1	-	1.2	1.0
Stand Pipe	1.5	-	1.2	1.0
Cable Tray	0.5	-	1.2	1.0
Pull Back Cylinders	0.5	-	1.2	1.0
Bell Nipple	2.0	-	1.2	1.2
Rat Hole Assembly	1.0	-	1.2	1.2
Tong Counter Weight Rails	0.6	-	1.2	1.2
Tong Block	0.05	-	1.2	1.2
Tong Counter Weight Bucket	0.5	-	1.2	1.2
Hydraulic Cathead	0.5	-	1.2	1.0
Ropes	3.5	-	1.2	1.0
Air Tank	0.3	-	1.2	1.0
Dead Line Anchor	1.2	-	1.2	1.0
Independent Rotary	12.0	-	1.2	1.5
Travelling Equipment	8.0	-	1.2	1.2

2.3.6.6.1.   Wind Velocity

According to the API 4F (2013), minimum design wind speeds for un-guyed masts are according to the Table 2.8:

Table 2.8: Minimum Design Wind Speed for Onshore Unguyed Mast, knots, V_{des}

Operating and Erection	Unexpected	Expected
32	60	75

However, design reference wind velocities, considered within this study, are according to the Table 2.9:

Table 2.9: Design Reference Wind Speed for Onshore Unguyed Mast, knots, V_{des}

Operating and Erection	Unexpected	Expected
40	70	95

In order to obtain the maximum rated design wind velocity (V_{des}), design reference wind speed should be multiplied by the Onshore SSL Multiplier (α_{onshore}) according to the Eq. (2.3).

$$V_{\text{des}} = V_{\text{ref}} \times \alpha_{\text{onshore}} \qquad (2.3)$$

In the above equation α_{onshore} is the Onshore Structural Safety Level Multiplier and is determined through the Structural Safety Level of E2 or U2 from Table 2.10. Local Wind Velocity is obtained by scaling the maximum rated design wind velocity by the appropriate Elevation Factor (β) using the Eq. (2.4).

$$V_z = V_{\text{des}} \times \beta \qquad (2.4)$$

where the value of β is obtained as follows:

$$\beta \begin{cases} \sqrt{0.85} & \text{height} \leq 15\text{ ft (4.6 m)} \\ \sqrt{2.01 \times \left({}^{z}/_{900}\right)^{0.211}} & \text{height} > 15\text{ ft (4.6 m)} \end{cases} \qquad (2.5)$$

in which z is the height above ground level for onshore drilling rigs or mean sea level for offshore drilling rigs.

Table 2.10: Onshore SSL Multiplier, α_{onshore} (API Specification 4F, 2013)

Case	Load Case	SSL	α_{onshore}	Approx. Return Period (years)
1a	Operating	All	1.00	N.A.
1b	Operating	All	1.00	N.A.
2	Expected	E2	1.00	50
3	Unexpected	U2	1.00	N.A.
4	Erection	All	1.00	N.A.
5	Transportation	All	1.00	N.A.

2.3.6.6.2.   Member by Member Wind Loading

The wind load applied on each member is acquired using the Eq. (2.6):

$$F_{\mathrm{m}} = 0.00338 \times K_i \times V_z^2 \times C_{\mathrm{s}} \times A \qquad (2.6)$$

where F_{m} denotes the wind force which is normal to the longitudinal axis of a member or normal to the surface of a wind wall or appurtenance and K_i represents the angle of inclination between the longitudinal axis of a member and wind direction, and is obtained through the Eq. (2.7):

$$K_{\mathrm{i}} = \sin^2 \phi \qquad (2.7)$$

where the angle of inclination of a member is illustrated in Figure 2.13.
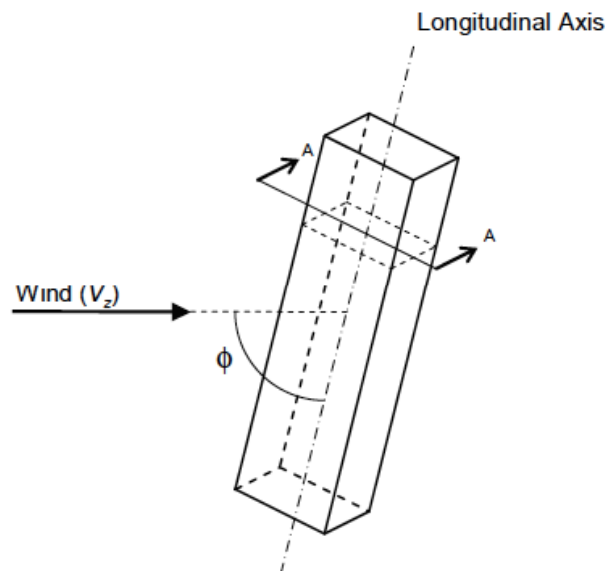
Figure 2.13. Member Angle of Inclination (API Specification 4F, 2013)

Moreover, V_z is local wind velocity in knots as discussed before, and C_s is the shape coefficient of the structural cross sections and is acquired from Table 2.11 according to the API 4F (2013). Likewise, A is the Projected Area of member and is obtained by multiplying the length of the member by the projected width, as demonstrated in Eq. (2.8):

$$A = L \times w \tag{2.8}$$

in which L and w denote the length and projected width of the structural member, respectively, and are illustrated in Figure 2.14.
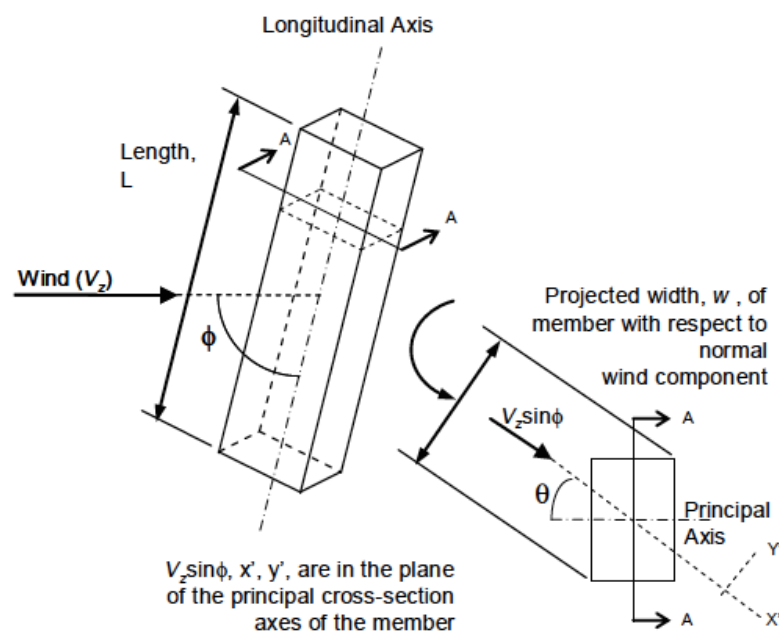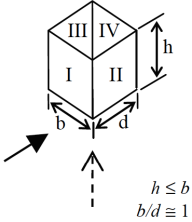
Figure 2.14. Member Projected Area (API Specification 4F, 2013)

Table 2.11: Shape Coefficients, C_s (API Specification 4F, 2013)

Section			Wind Orientation (θ)	C_s
Type	Shape			
Structural	Beams		All	1.8
	Built-up Members		All	2.0
Tubular	Square, Rectangular		All	1.5
	Round		All	0.8
Attachments	Any attachment with flat edges, such as travelling block and top drive		All	1.2
	Any attachment with a continuous surface, such as stand pipes and hoses		All	0.8
Wind Walls	Four-Sided, Airflow permitted into closure		$0^o \pm 20^o$ to normal	$I: 0.8$ $II: -0.5$ $III: -0.5$ $IV: -0.3$
			$45^o \pm 25^o$ to diagonal	$I: 0.5$ $II: 0.5$ $III: -0.5$ $IV: -0.5$

30

According to the API 4F (2013) standard, total wind load imposed upon the structure is obtained through the Eq. (2.9):

$$F_t = G_f \times K_{sh} \times \sum F_m \qquad (2.9)$$

where G_f represents the Gust Effect Factor which is only applied when calculating the total wind load on the structure. The value of gust effect factor is determined according to the Table 2.12. Moreover, K_{sh} refers to the factor accounting for global shielding effects and airflow changes around member or appurtenance ends. This factor is calculated according to Eq. (2.10) through utilizing the solidity ratio of the structure (ρ) which is calculated by dividing the projected area of all members in the front face of the bare frame by the projected area enclosed by the outer frame members normal to the wind direction.

$$K_{sh} = 1.11\rho^2 - 1.64\rho + 1.14;$$
$$0.5 \leq K_{sh} \leq 1.0 \qquad (2.10)$$

Table 2.12: Gust Effect Factor, G_f (API Specification 4F, 2013)

Gross Projected Area, m² (ft²)	G_f
>65 (700)	0.85
37.2-65 (400-700)	0.90
9.3-37.1 (100-399)	0.95
>9.3 (100)	1.00

Based on the Section 8.1.2 of the API Specification 4F (2013), for operating condition, the allowable unit stresses shall not be increased, while for the

unexpected and expected design storm conditions, allowable unit stresses may be increased by 33% over the basic allowable stresses.

2.3.6.7. Seismic Load

Section 8.5 of the API 4F (2013) addresses the Earthquake Loads imposed upon the drilling rig structures. This load case is not a dominant environmental load case in most regions of the world, since the drilling process is carried out in a short period of time and exposure of the structure to the seismic loads is considered unlikely. However, design of drilling rigs for seismic loads have recently been a routine procedure and for fixed offshore platforms the provisions of ISO 19901-2 (2017) are utilized. In land drilling rigs, though, the API Specification 4F (2013) does not provide the design methodology for seismic loads and refers to the local seismic design standards for the seismic analysis and design of rigs.

According to the Section 2.6 of Turkish Seismic Code, either the Mode Combination Method or the Time Domain Analysis Method shall be utilized for seismic analyses of structures taller than 40 m. Since the drilling rig being studied exceeds this limit, the Mode Combination Method is selected for the seismic analysis.

2.3.6.7.1. Elastic Spectral Coefficient Acceleration

The elastic spectral coefficient acceleration, which is equal to the ordinate of 5% damped elastic design acceleration coefficient is defined as follows:

$$S_{ae}(T) = A(T)g \tag{2.11}$$

where g denotes the acceleration of gravity and $A(T)$ represents the Spectral Acceleration Coefficient for seismic analysis per section 2.4 of the Turkish Seismic Standard and is defined as in Eq. (2.12):

$$A(T) = A_o \, I \, S(T) \tag{2.12}$$

where A_o, I, and $S(T)$ illustrate the Effective Ground Acceleration Coefficient, Building Importance Factor, and Spectrum Coefficient, respectively.

2.3.6.7.2.   Effective Ground Acceleration Coefficient

Since drilling rigs are machinery that have the possibility of operating in different locations during their lifetime, the most severe seismic zone should be considered in their seismic analyses. According to the Table 2.2 of Turkish Seismic Code, the effective ground acceleration coefficient for Seismic Zone 1, is taken as $A_o = 0.4$.

2.3.6.7.3.   Building Importance Factor

Considering the selection of medium consequences of failure for the structure by within this study, the Importance Factor is selected as $I = 1.2$ according to the Table 2.3 of Turkish Seismic Code.

2.3.6.7.4.   Local Site Class

Since drilling rigs are machinery that have the possibility of operating in different locations during their lifetime, a local site class with severe conditions should be considered for their seismic analysis. According to the Table 6.2 of Turkish Seismic Standard, the local site class is selected as Z3.

2.3.6.7.5.   Spectrum Coefficient

The spectrum coefficient is determined based on the spectrum characteristic periods as defined in Table 2.4 of Turkish Standard. For the local site class Z4, the following periods shall apply.

Table 2.13: Spectrum Characteristic Periods (Turkish Seismic Code 2007)

Local Site Class	T_A (Seconds)	T_B (Seconds)
Z3	0.15	0.60

2.3.6.7.6. Seismic Load Reduction Factor

According to the Table 2.8 of the Turkish Seismic Code (2007), for space truss steel towers, steel silos, and industrial chimneys with uniformly distributed mass along height, the structural behavior factor for non-building structures should be selected as 4. However, since according to the Table 12.2-1 of the ASCE 7 (2006), a minimum value of 3 is specified as R_a for steel systems not specifically detailed for seismic resistance, the more conservative value of 3 is selected for this study.

2.3.6.7.7. Participating Mass of the Rig System

Considering the major differences in loading of the drilling rigs, four different loading scenarios are considered for calculation of the participating mass in seismic loading (Turner et al. 2002). The loading scenarios are as follows:

- **Loading Scenario 1:** No hook load, no setback load, and Travelling Equipment at lowest position. This loading scenario represents the low natural period condition.

- **Loading Scenario 2:** 80% hook load, no setback load, and Travelling Equipment at highest position. Since the 100% rated hook load is considered an unlikely event, this loading scenario represents a high hook load case.

- **Loading Scenario 3:** No hook load, 100% setback load, and Travelling Equipment at highest position. This loading scenario represents the high natural period condition associated with full rated setback load.

- **Loading Scenario 4:** 50% hook load, 75% setback load, and Travelling Equipment at highest position. This loading scenario represents a prevalent combination of the hook load and setback load.
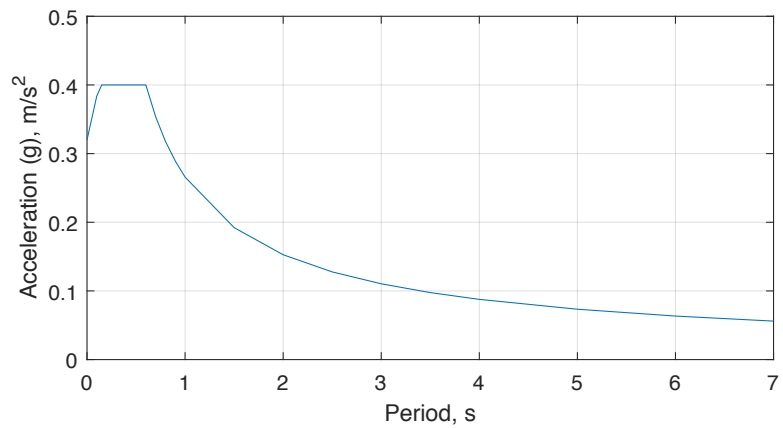
Figure 2.15. Special Design Acceleration Spectra

It should be noted that the setback mass is not completely located on the setback area and according to Turner et al. (2002), 55% of the setback mass is placed at the racking board and the remaining 45% is located on the setback area. Moreover, in seismic load combinations where both the hook and setback loads are present, a reduction factor is applied on these load cases since the possibility of having a drilling rig with the simultaneous full setback, rated static hook load, and design earthquake is highly unlikely and is not deemed an appropriate design condition. Moreover, a preference is given to the setback loads than the hook load, since it is present for a longer time and may govern the seismic design procedure. The interaction between the rated static hook load and the setback load can be demonstrated through the Figure 2.16. Moreover, the combinations are illustrated in Table 2.14. It should be mentioned that since the hook load does not contribute to the mass of the structure, its value is taken as zero.

2.3.6.7.8. Modal Load Cases

In employing the response spectrum method, the minimum number of modes accounting for 90% of the modal mass participation are included as provided in Table 6.9. Moreover, CQC method is utilized for the modal combination, while the

35

SRSS method employed for combining the directions. Additionally, modal damping ratio is set to 5% for all mode shapes.

2.3.6.7.9.   Allowable Stresses

Based on the Section 8.5 of the API Specification 4F (2013), the allowable stresses for the combined seismic, gravity, and operational loading may be increased by 33% over the basic allowable stresses.

2.3.6.8.   Temperature Load

As specified within this study, the maximum and minimum working environment temperatures are set to +50 and -30 °C, respectively.
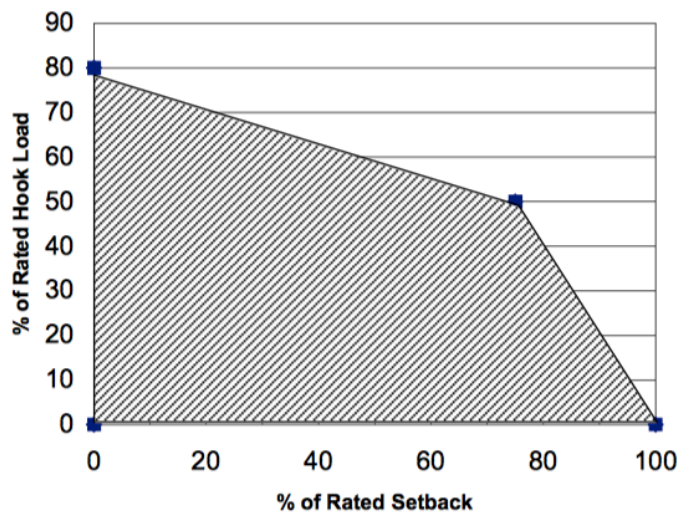
Figure 2.16. Seismic Design Interaction Cases (Turner et al. 2002)

Table 2.14: Mass Source Combinations

Mass Source	Load	Factor
Mass Source 1	Self-Weight	1.20
	Equipment Load (TE: Lowest Position)	1.20
	Hook Load	0
	Setback Load	0
Mass Source 2	Self-Weight	1.20
	Equipment Load (TE: Highest Position)	1.20
	Hook Load	0
	Setback Load	0
Mass Source 3	Self-Weight	1.20
	Equipment Load (TE: Highest Position)	1.20
	Hook Load	0
	Setback Load	1.00
Mass Source 4	Self-Weight	1.20
	Equipment Load (TE: Highest Position)	1.20
	Hook Load	0
	Setback Load	0.75

CHAPTER 3

STRUCTURAL DESIGN FORMULATION

3.1. Introduction

As mentioned in the initial chapter, every optimization problem is composed of an objective function, a set of design variables, and several design constraints. In structural engineering size optimization problems, design variables are usually a set of cross sections selected from a list of available sections. Design variables of a problem composed of N_m members are illustrated in Eq. (3.1):

$$\mathbf{I} = \left[I_1, I_2, \dots, I_{N_m}\right]^T \tag{3.1}$$

Correspondent to the cross-sectional areas as illustrated in Eq. (3.2):

$$\mathbf{A} = \left[A_1, A_2, \dots, A_{N_m}\right]^T \tag{3.2}$$

In the above equations, I is an integer value representing the sequence of the cross sections in a section list and A is a real value denoting the cross-sectional area of the relevant section. Values of A in Eq. (3.2) are obtained through the optimization process on the objective function, which is usually the weight of the structure as demonstrated in Eq. (3.3):

$$W = \sum_{i=1}^{N_g} \rho_i A_i \sum_{m=1}^{N_s} L_m \tag{3.3}$$

in which, ρ_i, A_i, and L_m illustrate the unit weight of the material, cross sectional area of the section assigned to the member group i, and length of the member m within group i respectively.

Optimization algorithms should satisfy the constraints imposed upon them, as well. For instance, in structural engineering problems, design constraints are strength and serviceability requirements of the relevant design standards. For steel structures, a variety of design standards including the LRFD-AISC (2016) can be utilized. However, according to the API 4F (2013), which is the main standard governing the analysis and design of the drilling structures, ASD-AISC (1989) should be employed for design of the steel drilling rigs. Thus, the analyses and design of the benchmark problems, as well as the onshore drilling rig are carried out based on the ASD-AISC (1989) specifications.

According to the ASD-AISC (1989), three main constraints including the slenderness, displacement, and strength requirements are usually taken into consideration. The requirements can be illustrated through the Eqs. (3.4), (3.5), and (3.6) respectively.

$$\left| \frac{\lambda}{\lambda_a} \right| - 1 \leq 0 \tag{3.4}$$

$$\left| \frac{\delta}{\delta_a} \right| - 1 \leq 0 \tag{3.5}$$

$$\left| \frac{f_a}{F_a} \right| - 1 \leq 0 \tag{3.6}$$

In Eq. (3.4), λ_a denotes the allowable slenderness ratio according to the ASD-AISC (1989) and is equal to 300 for members in tension and 200 for members in compression. Moreover, λ illustrates the slenderness ratio of structural members and is calculated according to the Eq. (3.7) as follows:

$$\lambda = \frac{Kl}{r} \tag{3.7}$$

In Eq. (3.7), K, l, and r denote the effective length factor of the member, unbraced length of the member, and radius of gyration of the structural section assigned to the corresponding member, respectively. Likewise, in Eq. (3.5), δ and δ_a indicate the displacement of the structural nodes and their allowable value, respectively. In addition, in Eq. (3.6), f_a and F_a typify the axial stress of the member and its allowable value respectively. In the following section, a summary of the strength requirements of Eq. (3.6) for steel trusses and frames according to the ASD-AISC (1989) is provided.

3.2. AISC 89 Requirements for Steel Trusses

According to the ASD-AISC (1989), for members in tension, the value of allowable axial stress shall not exceed $0.6F_y$ on the gross area nor $0.5F_u$ on the effective net area. For members in compression, though, the value of F_a is attained through a more sophisticated formula depending on the value of λ as in Eq. (3.7), as well as the value of C_c as in Eq. (3.8).

$$C_c = \sqrt{\frac{2\pi^2 E}{F_y}} \tag{3.8}$$

For the inelastic buckling case where the largest effective slenderness ratio of an element (λ) does not exceed the value of C_c, the allowable stress is determined through the Eq. (3.9).

$$F_a = \frac{[1 - \frac{\lambda^2}{2C_c^2}]}{\frac{5}{3} + \frac{3\lambda}{8C_c} - \frac{\lambda^3}{8C_c^3}} F_y \tag{3.9}$$

Conversely, for the elastic buckling case where the largest effective slenderness ratio of an element (λ) exceeds the value of C_c, Eq. (3.10) should be employed.

$$F_a = \frac{12\pi^2 E}{23(\frac{Kl}{r})^2} \tag{3.10}$$

41

3.3. AISC 89 Requirements for Steel Frames

According to the ASD-AISC (1989), the value of the computed stresses for a combination of tensile axial and bending stresses in any point along the length of the doubly and singly symmetrical members should satisfy the Eq. (3.11):

$$\frac{f_a}{0.6F_y} + \frac{f_{bx}}{F_{bx}} + \frac{f_{by}}{F_{by}} \leq 1.0 \qquad (3.11)$$

On the other hand, the value of computed stresses for a combination of compressive axial and bending stresses depends on the value of f_a/F_a.

For $f_a/F_a > 0.15$, the larger of Eqs. (3.12) and (3.13) applies.

$$\frac{f_a}{F_a} + \frac{C_{mx}f_{bx}}{\left(1 - \frac{f_a}{F'_{ex}}\right)F_{bx}} + \frac{C_{my}f_{by}}{\left(1 - \frac{f_a}{F'_{ey}}\right)F_{by}} \leq 1.0 \qquad (3.12)$$

$$\frac{f_a}{0.6F_y} + \frac{f_{bx}}{F_{bx}} + \frac{f_{by}}{F_{by}} \leq 1.0 \qquad (3.13)$$

and for $f_a/F_a \leq 0.15$, the following equation should be employed.

$$\frac{f_a}{F_a} + \frac{f_{bx}}{F_{bx}} + \frac{f_{by}}{F_{by}} \leq 1.0 \qquad (3.14)$$

In the aforementioned equations, f_a and f_b represent the computed axial and bending stresses respectively. Furthermore, F_y and F_b denote the yield stress of the material as well as the allowable bending stress, respectively. Moreover, F_a denotes the allowable axial stress under axial compressive force alone according to the Eq. (3.9) or (3.10). Additionally, F'_e represents the Euler Stress divided by a safety factor as in the Eq. (3.15).

$$F'_e = \frac{12\pi^2 E}{23\left(\frac{Kl_b}{r_b}\right)^2} \qquad (3.15)$$

where K and l_b represent the effective length factor and unbraced length in the plane of bending respectively and r_b denotes the radius of gyration. Moreover, C_m is a coefficient illustrating the distribution of moment along a member length. For compression members in sway frames C_m is equal to 0.85. However, for compression members which are rotationally restrained in non-sway frames and which are not subject to transverse loading between their supports in the plane of bending, the value of C_m ought to be calculated according to the Eq. (3.16):

$$C_m = 0.6 - 0.4 \left(\frac{M_1}{M_2} \right) \tag{3.16}$$

In which M_1/M_2 denotes the ratio of the smaller moment to the larger moment at the ends of the unbraced member in the plane of bending. Moreover, for compression members in non-sway frames which are also subject to transverse loading between their supports in the plane of loading, the allowable C_m values are as follows: For members whose ends are rotationally restrained in the plane of bending, the value is equal to 0.85, while for the unrestrained ones, the value shall be taken as 1.0.

CHAPTER 4

CONVERGENCE RATE INTEGRATED METAHEURISTIC SEARCH ALGORITHMS

4.1. Introduction

Metaheuristics have indisputably made the optimization of large-scale structural engineering problems possible. Compared to the traditional methods, they are easier to code and implement, and since they do not require the calculation of the gradient information of the objective function, they can be applied to discrete sizing optimization problems, as well. Their convergence towards the optimum solution and their overall efficiency when dealing with large scale problems, however, have been a matter of controversy. This is mostly due to the large number of structural analyses required to obtain a feasible solution in real world structural problems including truss roofs, truss domes, and especially in large-scale frame structures. Many endeavors have been carried out to tackle this drawback, some of which are outlined below.

Azad & Hasançebi (2015) and Azad et al. (2014) proposed a design driven approach to lower the computational effort of the optimization in frames and trusses. In this method, loading capacity of each structural member (strength requirement), as well as the contribution of each structural member to the total displacement in each direction (displacement constraint) are considered as the member-wise information to lead the search direction of the algorithm in an efficient way. However, complexities in coding and implementation of the aforementioned strategy should be weighed against the advantages provided by this method.

Later on, Hasançebi et al. (2011) recommended employing the parallel computing method with a cluster computing system of 32 processors for optimizing the high rise steel buildings. Through this method, three high rise steel buildings using (ASD-AISC, 1989) standard and actual loading are analyzed and a maximum speed up ratio of about 16 is achieved in the analyses. In a recent study, Khatibinia & Yazdani (2018) amalgamated the simplex crossover and breeder genetic algorithm into the multi-gravitational search algorithm to increase its exploration and exploitation capabilities. While achieving better objective function values through analyzing four truss examples, the new accelerated multi-gravitational search algorithm demonstrated less computational effort compared to the former version, as well. Moreover, Kaveh & Ghazaan (2016) have merged the Enhanced Colliding Bodies Optimization into the Upper Bound Strategy, resulting in an algorithm maintaining both the efficiency and the accuracy. Taking all the efforts into consideration, a new method for reducing the computational cost yet maintaining the optimum weight quality is outlined below.

4.2. Convergence Rate

Convergence Rate is an approach which enhances the efficiency of the metaheuristics in dealing with the large-scale structural engineering problems by reducing the required computational effort to reach an optimum solution. The rationale behind this approach can be traced back to the convergence of the objective function of the optimization problems towards an optimum solution. According to Figure 4.1, since objective function diagrams of almost any optimization problem follow quite a smooth path towards the optimum solution, one can make a rough estimation on the probable value of the objective function of the next iteration using the objective function values of the former iterations.

Through this approach, once the objective function value of an individual calculated by the structural analyses in any iteration surpasses the expected objective function value calculated by a simple mathematical procedure, the analyses of the remaining individuals within the same population are skipped. In fact, since the objective

function value of the remaining individuals will most probably fall within the immediate vicinity of the expected value and no sharp drops in the objective function diagram will occur, the increase in the efficiency of the algorithm through this approach is preferred over the analyses of the remaining individuals and obtaining the probably improved results. The expected value of the objective function is calculated according to the Eq. (4.1):
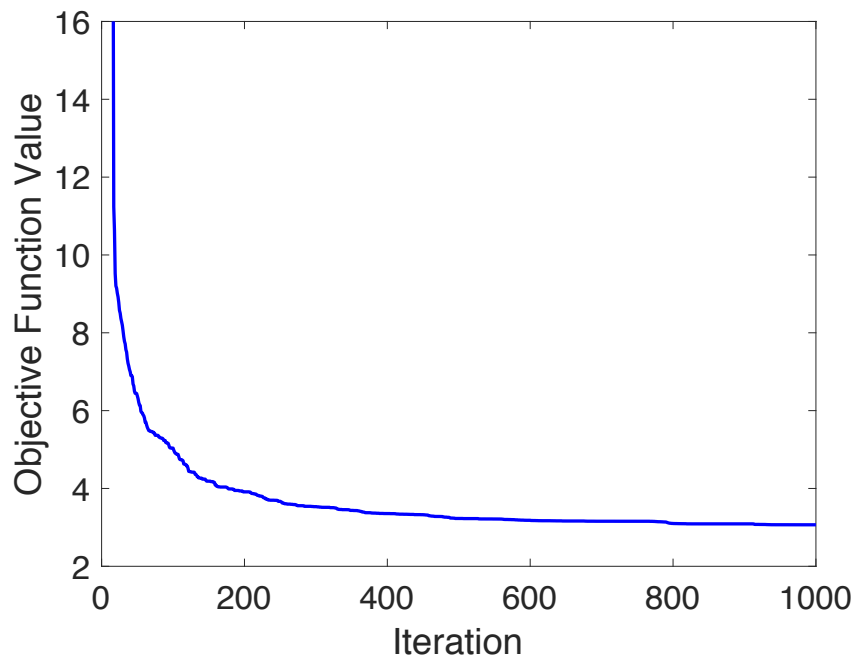
Figure 4.1. Schematic View of the Objective Function Graph

$$Expected\ Objective\ Function\ Value(it) = f\left(I_{best}^{it-1}\right) - \frac{CRC}{RMF} \times \left\{ f\left(I_{best}^{it-(RMF+1)}\right) - f\left(I_{best}^{it-1}\right) \right\} \quad (4.1)$$

In Eq. (4.1), $f\left(I_{best}^{it-1}\right)$ and $f\left(I_{best}^{it-(\mathrm{RMF}+1)}\right)$ denote the best objective function values obtained in iterations $(it-1)$ and $it-(\mathrm{RMF}+1)$, respectively. Moreover, in the above equation, CRC is the Convergence Rate Coefficient which can take any positive real values. Additionally, Rate Modification Factor (RMF) is utilized for determination of the number of required iterations for the algorithm to calculate the average value of decrease in the objective function.
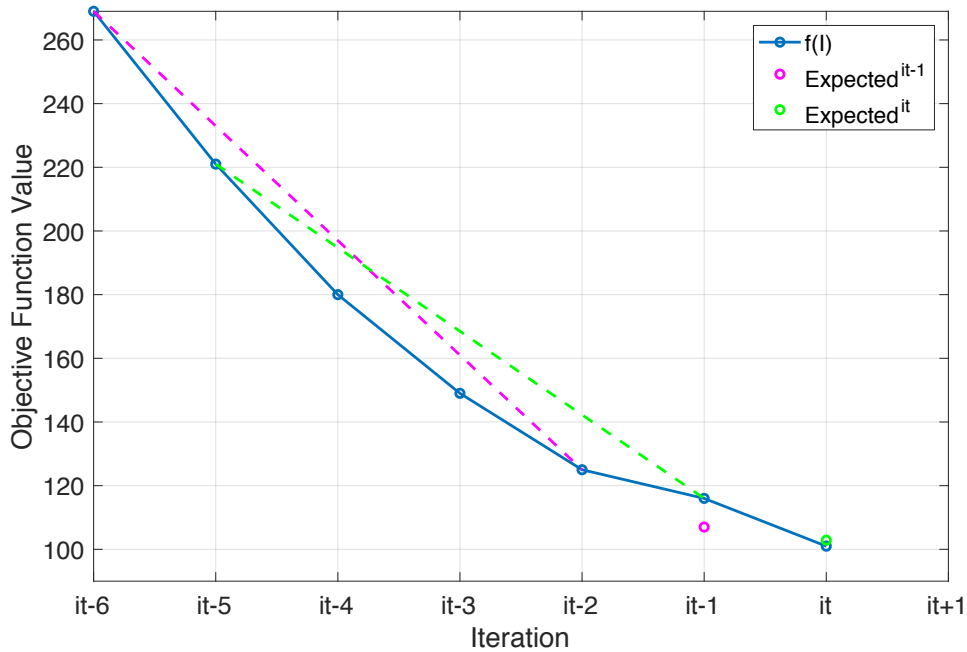
Figure 4.2. Convergence Rate Algorithm

As depicted in the Figure above, if the algorithm succeeds in finding an objective function value lower than the expected value in iteration $(it-1)$, the rest of the analyses will be skipped. However, if neither of the individuals lie below the estimated value, as shown with a pink circle in the Figure above, no savings in the

48

number of the analyzed candidates will be achieved and structural analyses continue to the next iteration. Therefore, value of the expected objective function will be calculated using the objective function values of iterations $(it - 5)$ and (it), as shown with a green circle, and a comparison will be made between the value of the expected and calculated objective functions.

Moreover, the expected objective function value is calculated according to the average decrease in the value of the objective functions during the last (RMF) iterations, which are indicated with the pink and green dashed lines. The pseudo code of the convergence rate method is outlined below:

1.	$f\left(\boldsymbol{I}_{best}^{it-1}\right) = W\left(\boldsymbol{I}_{best}^{it-1}\right) \times \left\{1 + Penalty\left(\boldsymbol{I}_{best}^{it-1}\right)\right\}$
2.	*while* $it \leq it_{max}$
3.	*generate offspring* $\left(\boldsymbol{I}_i^{it}, i = 1:\lambda\right)$ *from elite* $\left(\boldsymbol{I}_{best}^{it-1}\right)$
	Expected Objective Function Value
4.	$= f\left(\boldsymbol{I}_{best}^{it-1}\right) - CR \times \left\{\dfrac{f\left(\boldsymbol{I}_{best}^{it-1-RMF^{it}}\right) - f\left(\boldsymbol{I}_{best}^{it-1}\right)}{RMF^{it}}\right\}$
5.	*for* $i = 1:\lambda$
6.	*Calculate* $f\left(\boldsymbol{I}_i^{it}\right)$
7.	*if* $f\left(\boldsymbol{I}_i^{it}\right) \leq$ *Expected Objective Function Value*
8.	*Skip Analyzing Rest of the Candidates*
9.	*end*
10.	*end*
11.	*Determine* $\boldsymbol{I}_{best}^{it}$ *and* $f\left(\boldsymbol{I}_{best}^{it}\right)$
12.	*end*

4.3. Upper Bound

Proposed by Azad et al. (2013), Upper Bound (UB) strategy has proven promising outcomes in lowering the required number of the structural analyses in order to

reach an optimum solution within the search space. The simplicity of the model, as well as its ease of implementation in $(\mu + \lambda)$ type metaheuristic algorithms have made it a reliable solution in tackling one of the downsides of the metaheuristics.

Generally, $(\mu + \lambda)$ type metaheuristics consist of μ parents and λ offspring. At every iteration of the algorithm, μ parents generate λ offspring, making the total population equal to $(\mu + \lambda)$. Then, the elitism rule is carried out by selecting the fittest individual to shrink the population to the μ best solutions as parents. Subsequently, these parents generate new offspring and this cycle continues until a termination criterion has been met. It should be mentioned that μ is generally taken as 1.

Normally, structural analyses are carried out on the individuals of the population and their penalized weight and fitness values are determined. Employing the Upper Bound strategy, however, differs from the normal approach slightly such that before performing the structural analysis, the net weight of the structure is calculated through the Eq. (3.3). Having the penalized weight of the parent individual as an upper limit, as well as the net weight of the offspring, one can determine that the offspring whose net weight is heavier than the penalized weight of the parent individual, has no chance in surpassing the parent individual's penalized weight, especially after the penalty value is added to their net weight.

This method improves the efficiency of the optimization process since it dramatically reduces the number of required structural analyses and thus, refrains from spending time on forming and solving the stiffness matrix of the structure for the individuals who have no chance of survival within the same population. Instead, it assigns a very large number to the penalty function of the aforementioned incompetent individuals and as a result, the individual is eliminated having the least fitness value in the population. The pseudo code for the UB method is as according to the next page.

```
1.    $f(I_{best}^{it-1}) = W(I_{best}^{it-1}) \times \{1 + Penalty(I_{best}^{it-1})\}$

2.    $while\ it \leq it_{max}$

3.        $generate\ offspring\ (I_i^{it}, i = 1:\lambda)\ from\ elite\ (I_{best}^{it-1})$

4.        $for\ i = 1:\lambda$

5.            $Calculate\ W(I_i^{it})$

6.            $If\ W(I_i^{it}) \leq f(I_{best}^{it-1})$

7.                $Calculate\ Penalty(I_i^{it})$

8.                $f(I_i^{it}) = W(I_i^{it}) \times \{1 + Penalty(I_i^{it})\}$

9.            $else$

10.                $Penalty(I_i^{it}) = infinity$

11.                $f(I_i^{it}) = W(I_i^{it}) \times \{1 + Penalty(I_i^{it})\}$

12.            $end$

13.        $end$

14.        $Determine\ I_{best}^{it}\ and\ f(I_{best}^{it})$

15.    $end$
```

where I_{best} and I_i refer to the elite and offspring in a population respectively, $f(I)$ represents the penalized weight of the individuals, and λ illustrates the number of individuals in a population. Additionally, it and it_{max} refer to the iteration number and maximum number of iterations respectively.

4.4. Formulation of the Adaptive Dimensional Search Algorithm

Initially introduced by Hasançebi & Azad (2015), Adaptive Dimensional Search algorithm employs the Search Dimensionality Ratio (SDR) parameter to generate the new candidate solutions from the elite. This method is in contrast with the prevalent theory in metaheuristics that an algorithm is usually inspired by a natural phenomenon.

Search dimensional ratio is the percentage of the design variables exposed to probabilistically perturbation through the new candidate solution generation and can be illustrated through the Eq. (4.2):

$$SDR = \frac{N_p}{N_d} \tag{4.2}$$

where N_p refers to the number of design variables perturbed and N_d represents the number of design variables in total. The value of SDR, of course, is restricted by a maximum and a minimum value. This restriction is imposed upon the value of SDR since an unjustifiably large SDR value may lead to an excessive perturbation, resulting in a slow convergence towards the optimum solution. Minimum value, however, is imposed upon this parameter to ensure that at least a minimum number of design variables, which is equal to one in this study, are perturbed and the offspring are in no way identical to the elite. The value of SDR is constrained as follows:

$$\frac{1}{N_d} \leq SDR \leq 0.5$$

Moreover, the initial value of SDR is taken as 0.25 and it is modified based on the structural analysis results of the previous iteration such that if the objective function value of the previous iteration is improved, the value of SDR is increased, leading the algorithm towards an explorative search. Otherwise, the value of SDR is decreased, guiding the algorithm through an exploitative search. This approach is similar to the structural engineering design style, where a limited number of design variables are modified, and the outcome of the subsequent structural analyses is utilized in modification approach through the next iteration. The optimization procedure through this method can be outline as follows:

Step 1. Initial Population: The initial population consisting of a specific number of random individuals is generated.

Step 2. Evaluation: The generated population undergoes the necessary structural analysis procedures using the relevant design standards, considering the displacement and stress constraints. The objective function values of the feasible solutions with no constraint violations are calculated according to the Eq. (3.3). In case a candidate solution violates the constraints imposed upon it, its objective function value will be penalized through the Eq. (4.3).

$$f = W + W * p(\Sigma_i c_i)$$ (4.3)

where f denotes the penalized objective function value, W symbolizes the pure weight of the structure, p is an optional value for adjusting the penalty value, and c_i represents the ith violated constraint.

Step 3. Setting the ADS Parameter: Through this step, the value of the Search Dimensionality Ratio is updated according to the Eq. (4.4). For the initial iteration, this value was set to 0.25; for the consequent iterations, however, its value is updated based on the values of the objective functions through the iterations $(it - 1)$ and $(it - 2)$ as follows:

$$SDR^{it} = \begin{cases} \dfrac{SDR^{it-1}}{\lambda} & f(I_{best}^{it-1}) < f(I_{best}^{it-2}) \\ \lambda \times SDR^{it-1} & f(I_{best}^{it-1}) = f(I_{best}^{it-2}) \end{cases}$$ (4.4)

In the equation above, if the value of the objective function in the previous iteration is improved compared to its value in iteration $(it - 2)$, the value of the SDR will be divided by the λ factor, which is called the search dimensional adaptation parameter. This factor is set to 0.98 within this study. Therefore, an increase in the value of the SDR will occur, and more individuals within a population will be perturbed resulting in a more explorative search. Otherwise, if the algorithm cannot

find an improved solution, the value of SDR will be multiplied by the λ factor, and a reduced SDR value will result in a more exploitative search within the search space.

Step 4. Generating the New Population: Once the value of SDR is determined, generation of the new candidates is carried out according to the Eq. (4.5):

$$I_{i,j}^{it} = \begin{cases} I_{i,best}^{it-1} & r_{i,j}^{it} > SDR \\ I_{i,best}^{it-1} + round\left[N_{i,j}^{it}(0,1) \times \left\{C - (C-1) \times \dfrac{it}{it_{max}}\right\}\right] & r_{i,j}^{it} \leq SDR \end{cases} \quad (4.5)$$

$$C = \sqrt{\left(I_i^{max} - I_i^{min}\right)} \quad (4.6)$$

where N(0,1) represents a standard normal distribution number with mean and standard deviation equal to zero and one respectively, and $r_{i,j}^{it}$ is a uniform random number between zero and one. Moreover, the value of C is illustrated in Eq. (4.6). A comparison between the value of SDR^{it} and $r_{i,j}^{it}$ determines whether the value of individual i within the population j should be directly copied from the elite or a new value should be assigned to it according to the Eq. (4.5).

Step 5. Elitism: The best design hitherto achieved is stored in a separate memory cell and is employed for generating the new candidate solutions according to the Eq. (4.5). Subsequent to the analyses of the newly generated candidate solutions, a comparison is carried out between the objective function of the candidate solutions obtained through the current iteration and the objective function of the best design acquired so far. If the best design is outperformed by any of the new candidate solutions, it is then replaced by the best solution obtained within the current iteration. Otherwise, if the best design obtained so far could not be surpassed by any of the new candidate solutions, then it retains its position in that specific memory cell. In the end, a design solution stored in the memory cell specific to the best design till the current iteration becomes responsible for the generation of the new candidate solutions for the next iteration.

Step 6. Stagnation Control: In case the algorithm is stagnated within a predefined number of iterations, the stagnation control strategy outlined through the last section of this chapter should be applied.

Step 7. Termination: Till the termination criterion is not met, which is usually the number of iterations, the algorithms reverts to the second step.

4.5. Formulation of the Exponential Big Bang-Big Crunch Algorithm

Inspired by the theory of the evolution of universe, the Big Bang-Big Crunch algorithm was initially proposed by Erol & Eksin (2006). In this theory, Big Bang refers to the energy dissipation and the consequent disorder which is simulated by generating some random points within the search space; Big Crunch, however, refers to the gravitational attraction of disordered particles which is imitated by calculating the center of mass of the random particles in iteration it, according to the Eq. (4.7):

$$I_{i,best}^{it} = \frac{\sum_{j=1}^{\lambda} \left\{ \frac{1}{f(I_j^{it})} \times I_{i,j}^{it} \right\}}{\sum_{j=1}^{\lambda} \frac{1}{f(I_j^{it})}} \tag{4.7}$$

where $I_{i,j}^{it}$ represents the ith component of the candidate solution j, produced in it^{th} iteration, and f denotes the objective function value of the candidate solution. Moreover, λ resembles the size of population generated during the big bang phase. Notwithstanding the equation above, the individual with the least penalized objective function value can also be selected as the elite instead of calculating the center of mass of the population.

Moreover, in each iteration, the offspring are produced from the elite according to the Eq. (4.8):

$$I_{i,j}^{it} = I_{i,best}^{it-1} + \frac{\alpha \times N_{i,j}^{it}(0,1)}{it} \times (I_i^{max} - I_i^{min}) \tag{4.8}$$

55

where $I_{i,best}^{it-1}$ denotes the center of mass of candidates in iteration $(it-1)$; I_i^{max} and I_i^{min} represent the upper and lower boundaries of the search space respectively; $N_{i,j}^{it}$ denotes a normal random number with a mean value and standard deviation of zero and one respectively, and α designates a fixed number taken equal to 0.5 within this study. Decreasing the normal random number through dividing it by the iteration number ascertains better results (Erol & Eksin, 2006).

Since the formulation of this method, it has been widely employed in locating the optimum solution of various engineering problems. Kaveh & Talatahari (2009b) employed this method in several truss optimization problems with results outperforming the Genetic Algorithm and Particle Swarm Optimization Method. A hybrid form of the BB-BC method has been utilized for designing the site layout for caisson structure fabrication (Prayogo et al. 2018). This method has also illustrated promising results in parameter estimation in structural systems (Tang et al. 2010).

Nonetheless the established robustness and stability of this method, some modifications have been carried out on this method to increase its efficiency and convergence towards the optimum solution. In fact, despite the satisfactory performance of the BB-BC algorithm in exploiting the search space around the local optimum point, there are some deficiencies in exploration capabilities of the method (Kaveh & Talatahari, 2010). In Particle Swarm Optimization method, which is inspired by the social interaction of bird flocking and fish schooling, individuals of a population adjust their movements within the search space according to their own experience, as well as the population's experience (Kennedy et al. 2001). Besides the intrinsic feature of the Big Bang-Big Crunch algorithm of calculating the center of mass of a population, the aforementioned characteristic of the Particle Swarm Optimization is integrated into the Big Bang-Big Crunch algorithm to improve its efficiency in finding the global optimum solution (Kaveh & Talatahari, 2009b).

Moreover, Alatas (2011) has proposed the Uniform Big Bang–Chaotic Big Crunch (UBB-CBC) algorithm to improve the exploration quality of the BB-BC algorithm

56

and to prevent it from being trapped in a local optimum. Later, Hasançebi & Azad (2014) proposed a refined version of the BB-BC algorithm named as the Modified Big Bang-Big Crunch (MBB-BC) algorithm by modifying the search dimensionality and step size. They addressed the shortcomings of the original algorithm by employing the nth power of the normal random number as illustrated in Eq. (4.9):

$$I_{i,j}^{it} = I_{i,best}^{it-1} + \frac{\alpha \times \left(N_{i,j}^{it}(0,1)\right)^{n}}{it} \times (I_i^{max} - I_i^{min}) \tag{4.9}$$

where the value of n is taken equal to 3. By utilizing the nth power of the normally distributed random number, search dimensionality is diminished at the beginning of the search process and is increased towards the final stages compared to the standard code. That being said, a steadier transition is experienced from the explorative search in the initial stages towards the exploitative search in the final stages. Since a large dimensionality ratio increases the randomness of the search process in discrete structural optimization and therefore decelerates the convergence of the algorithm, this modification leads to an increase in the efficiency of the algorithm. Moreover, increased values of SDR in the final stages prevents the search process from being restricted to a limited search space. On the other hand, the nth power of the normally distributed random number paves the way for a haphazard increase of the step size in the final stages of the optimization process for values of normally distributed number which are greater than one. Thus, entrapment of the algorithm in a local optimum point in the final iterations is prevented by increasing the exploration ability of the algorithm.

In another study by Hasançebi & Azad (2012), the normally distributed number is replaced by an exponentially distributed number with a mean value and variance of $1/\lambda$ and $1/\lambda^2$, respectively, as illustrated in Eq. (4.10). In this algorithm, which is named the Exponential Big Bang-Big Crunch (EBB-BC) algorithm, the initial value of λ is taken as one; however, if all the design variables in an individual are

identical to the parent individual, its value is divided by two and this process continues until a different offspring is produced.

$$I_{i,j}^{it} = I_{i,best}^{it-1} \pm \frac{\alpha \times \left(E_{i,j}^{it}(\lambda = 1)\right)^{n}}{it} \times (I_i^{max} - I_i^{min}) \qquad (4.10)$$

Since the EBB-BC is a refined and steadier version of the MBB-BC algorithm, it is utilized in the following chapters. The optimization procedure through this method can be outline as follows:

Step 1. Initial Population: The initial population consisting of a specific number of random individuals is generated.

Step 2. Evaluation: The generated population undergoes the necessary structural analysis procedures using the relevant design standards, considering the displacement and stress constraints. The objective function values of the feasible solutions with no constraint violations are calculated according to the Eq. (3.3). In case a candidate solution violates the constraints imposed upon it, its objective function value will be penalized through the Eq. (4.3). Afterwards, fitness value of the candidate solutions will be calculated either through the 1/W for feasible solutions or 1/f for infeasible solutions and will be apportioned to the mass values of the individuals.

Step 3. Big Crunch Phase: Center of mass of the individuals within the population is calculated through the Eq. (4.7). Moreover, the fittest value within the population having the greatest mass can also be selected as the center of mass of the population instead of employing the aforementioned burdensome equation.

Step 4. Big Bang Phase: Generation of the new candidate solutions is carried out according to the Eq. (4.10). This equation employs the exponential distribution with a mean value of $1/\lambda$ and a variance of $1/\lambda^2$ for the generation of the new

58

individuals. The value of λ may be decreased in case the algorithm fails to generate a candidate solution unlike the parent individual.

The probability density function of the exponential distribution is according to the Eq. (4.5) and its shapes for various λ values are plotted in Figure 4.3.

$$f(x; \lambda) = \begin{cases} \lambda e^{-\lambda x} & x \geq 0 \\ 0 & x < 0 \end{cases} \tag{4.11}$$

It is worth mentioning that this function only produces positive numbers. Thus, a haphazard positive or negative sign should be applied in Eq. (4.10) to allow either for an increase or a decrease in the value of a design variable.

Moreover, the value of λ, which is initially set to 1.0, may be subject to a division by 2 once the algorithm fails to generate an individual different from the parent individual. Therefore, according to the Figure 4.3, a decreased value of λ will yield to a smoother probability distribution curve, resulting in larger step sizes. This process continues until a different individual from the parent individual is produced. Afterwards, the value of λ is reset to 1 for the generation of the next individual.

Step 5. Elitism: The best design hitherto achieved is stored in a separate memory cell and is employed for generating the new candidate solutions according to the Eq. (4.10). Subsequent to the analyses of the newly generated candidate solutions, a comparison is carried out between the objective function of the candidate solutions obtained through the current iteration and the objective function of the best design acquired so far. If the best design is outperformed by any of the new candidate solutions, it is then replaced by the best solution obtained within the current iteration. Otherwise, if the best design obtained so far could not be surpassed by any of the new candidate solutions, then it retains its position in that specific memory cell. In the end, a design solution stored in the memory cell specific to the best design till the current iteration becomes responsible for the generation of the new candidate solutions for the next iteration.

Figure 4.3. PDF of Exponential Distribution

Step 6. Stagnation Control: In case the algorithm is stagnated within a predefined number of iterations, the stagnation control strategy outlined through the last section of this chapter should be applied.

Step 7. Termination: Till the termination criterion is not met, which is usually the number of iterations, the algorithms reverts to the second step.

4.6. Stagnation Control Strategy

One of the efficient strategies in backing the algorithm to escape the local optimum point traps is outlined in Hasançebi & Azad (2015). Three different strategies are addressed including Uphill Move, Annealing, and Penalty Relaxation strategies. In this study, though, the Uphill Move Strategy is selected and integrated into the

optimization algorithm, since according to the literature, it provides more promising results compared to the other strategies.

In uphill move strategy, if the objective function of an algorithm does not improve in a specified number of iterations, for instance 20 iterations, an uphill move is carried out such that the new offspring is produced from an individual within the population having the objective function value less than a percentage of the objective function value of the elite as in Eq. (4.12).

$$f(I_{Elite})_{\text{temp}} \leq \alpha \times f(I_{Elite}) \qquad (4.12)$$

Therefore, instead of the (I_{Elite}), $(I_{Elite})_{\text{temp}}$ is utilized in Eqs. (4.5) and (4.10) to generate the new offspring for the next iteration. In current study, the value of α is taken as 102%, since smaller and larger values may lead to individuals with undesirable outcomes.

A new period which is named as the "Stagnation Escape Period" (SEP) is defined and through this period, which is again taken as 20 iterations in the present study, if any offspring result in an objective function value less than the objective function value of the $f(I_{Elite})_{\text{temp}}$, then the new individual replaces the $(I_{Elite})_{\text{temp}}$ and the new $(I_{Elite})_{\text{temp}}$ produces the offspring for the next iteration. This process continues until the Stagnation Escape Period reaches the maximum value specified. However, if the $f(I_{Elite})_{\text{temp}}$ succeeds in reaching a value less than the $f(I_{Elite})$, then the process is terminated before the SEP reaches the maximum value. Conversely, if $f(I_{Elite})_{\text{temp}}$ fails to outdo the $f(I_{Elite})$ within the specified maximum SEP, a new SEP starts with the uphill move with reference to the last $f(I_{Elite})_{\text{temp}}$ of the previous SEP as demonstrated in Eq. (4.13).

$$f(I_{Elite})_{\text{temp}(current\ SEP)} \leq \alpha \times f(I_{Elite})_{(previous\ SEP)} \qquad (4.13)$$

Moreover, the value of α can also be subject to a slight increase in this new SEP. This process continues until the $f(\boldsymbol{I}_{Elite})_{\text{temp}}$ surpasses the $f(\boldsymbol{I}_{Elite})$ and the algorithm escapes from the local optimum solution.

CHAPTER 5

VERIFICATION OF CONVERGENCE RATE INTEGRATED METAHEURISTIC SEARCH ALGORITHMS

5.1. Introduction

Through this section, three truss examples are analyzed with the Convergence Rate approach integrated ADS and EBB algorithms. Value of Convergence Rate Coefficient (CRC) and Rate Modification Factor (RMF) are set to 0.1 and 10, respectively. The rationale behind the selection of 0.1 for CRC will be explained in the following sections. Furthermore, in order to avoid being trapped in the local optimum solutions, the examples are run for 10 times and the stagnation control strategy with an allowable uphill move of 2% and Stagnation Escape Period (SEP) of 20 is integrated into the algorithms.

As formulated in the previous chapter, structural analyses are carried out according to the ASD-AISC (1989). likewise, circular hollow sections are selected according to the aforementioned standard as illustrated in Table 5.1. The yield stress, modulus of elasticity, and unit weight of the steel material are set to 248.2 MPa, 200 GPa, and 7.85 gr/cm^3, respectively. Moreover, from the three real-world problems, 117-Bar Truss example is taken from Azad (2017), and 130-Bar and 392-Bar Truss examples are taken from Azad et al. (2014). Detailed explanation of these examples is provided within the following sections.

5.2. 117-Bar Cantilever Truss Example

The first problem is a steel cantilever truss with 117 members and 30 joints as depicted in Figure 5.1. The members are not grouped, and the optimization is carried out on each member of the truss, individually. Furthermore, the truss is

loaded by three distinct load cases. In load cases 1, 2, and 3, joint loads of 15 kN are applied to all unsupported nodes in the x, y, and -z directions, respectively, and the self-weight of the structure is neglected. Additionally, displacement of the truss tip is restricted to 40 mm in all directions. For this problem, the population size and maximum number of iterations are set to 50 individuals and 1000 iterations, respectively.

Though the number of individuals can have different values including 5, 10, and 20, the selected value of 50 has given the best results according to the numerous tests and is used within this study. Moreover, since most of the individuals within a population are not analyzed due to the application of the Convergence Rate approach, small values for the number of individuals may not be enough.

Table 5.1: Circular Hollow Section List

Section No	Section Name	Area, mm²	Section No	Section Name	Area, mm²	Section No	Section Name	Area, mm²
1	P.5	161.3	14	P3	1438.7	27	PXX4	5225.8
2	PX.5	206.5	15	PX2.5	1451.6	28	P8	5419.3
3	P.75	214.8	16	PXX2	1716.1	29	PX6	5419.3
4	PX.75	279.4	17	P3.5	1729.0	30	PXX5	7290.3
5	P1	318.7	18	PX3	1948.4	31	P10	7677.4
6	PX1	412.3	19	P4	2045.2	32	PX8	8258.1
7	P1.25	431.6	20	PX3.5	2374.2	33	P12	9419.3
8	P1.5	515.5	21	PXX2.5	2600.0	34	PXX6	10064.5
9	PX1.25	568.4	22	P5	2774.2	35	PX10	10387.1
10	P2	690.3	23	PX4	2845.2	36	PX12	12387.1
11	PX1.5	690.3	24	PXX3	3529.0	37	PXX8	13741.9
12	PX2	954.8	25	P6	3600.0			
13	P2.5	1096.8	26	PX5	3941.9			
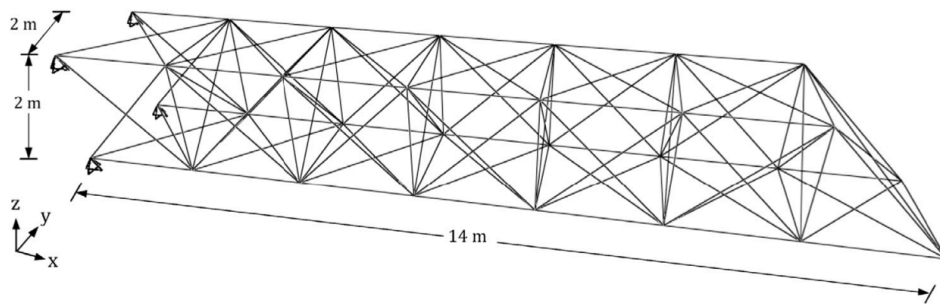
Figure 5.1. 117-Bar Cantilever Truss (Azad 2017)

Through this study, prior to operating the analyses concerning the performance of the Converge Rate approach compared to the Upper Bound strategy integrated metaheuristics, some analyses regarding the sensitivity of the Convergence Rate approach to the various CRC values are carried out. Six different real numbers are assigned to the CR approach, and the analyses are run for a specific number of analyzed individuals. Moreover, in order to have a better decision on the suitability of the CRC values, analyses are run for five times and the analysis having the best objective function value is chosen for comparison between the CRC values.

As illustrated in Figure 5.2, the CRC value of 0.1 illustrates the fastest convergence towards the optimum solution compared to the other five coefficients. Moreover, as the value of CRC increases, the convergence rate of the algorithm towards the optimum solution declines. Therefore, a CRC value of 0.1 is employed for the rest of the analyses throughout this study.
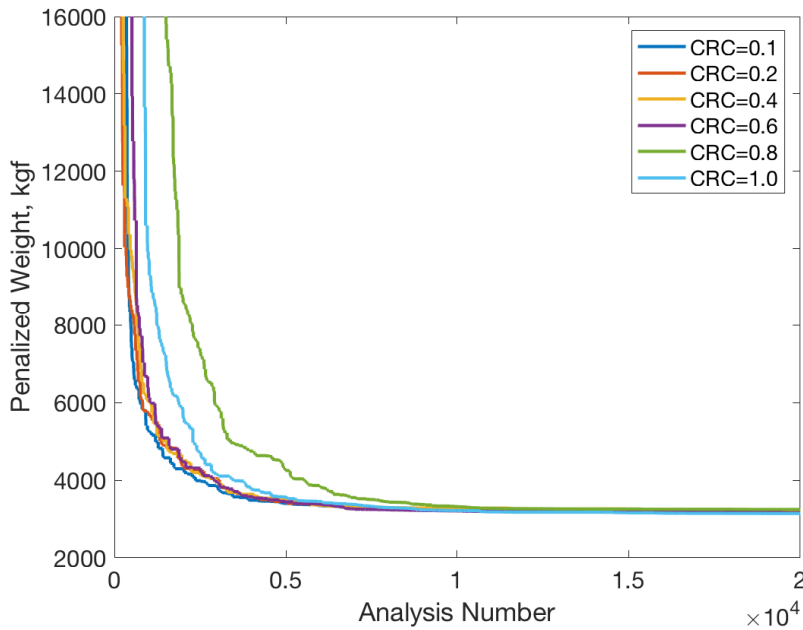
Figure 5.2. Convergence History in 117-Member Truss for Various CRC's

According to the Table 5.2, for the Convergence Rate approach integrated ADS algorithm a design weight of 3200.15 kgf and for the Upper Bound integrated ADS algorithm a design weight of 3254.97 kgf are obtained. Furthermore, for EBB algorithm, design weight values for the aforementioned approaches are equal to 3129.03 kgf and 3098.19 kgf, respectively. Additionally, CR approach surpasses the UB approach in terms of the saved analyses in both ADS and EBB algorithms. In ADS metaheuristic method, percentage of the saved analyses is 65% for CR and 49% for UB approaches. Likewise, for EBB algorithm, these values are equal to 65% and 58% for CR and UB strategies, respectively. An enhancement in terms of the computational time of the CR integrated metaheuristic algorithms, compared to the UB integrated methods, is observed, as well. For instance, the computational time of 153 s for the UB integrated ADS method is obtained; this value, however, is reduced to 108 s for the CR integrated ADS method. The same trend is visible in CR and UB integrated EBB algorithms, as well.

66

Moreover, according to the Table 5.2, mean weight values acquired within this study are not affected by the Convergence Rate approach compared to the mean weight values within the literature. Furthermore, the proposed method demonstrates a better performance in lowering the number of required structural analyses compared to those of the UB as well as the guided methods.

According to the Figure 5.3, though the CR algorithm precludes a vast majority of the candidates from being analyzed, it is still converging to the optimum solution without being trapped in a local optimum point. The reason for this phenomenon can be traced back to the selection of the appropriate convergence rate coefficient as well as a suitable rate modification factor so that a reasonable decrease in the value of the objective function is expected through the optimization process as illustrated in Figure 5.4. As it can be perceived form this figure, the expected decrease in the value of the objective function, lies well below the real decrease in the value of the objective function in CR and UB approach integrated algorithms. Moreover, Figure 5.5 illustrates the structural analyses savings of the CR integrated metaheuristic algorithms throughout the structural optimization process, which demonstrates a massive number of candidate solutions disqualified from being analyzed.

Table 5.2: Optimum Design Results for 117-Member Cantilever Truss

	ADS		EBB		ADS*	EBB*	GADS*	GEBB*	GADS-EBB*
	CR	UB/Standard	CR	UB/Standard	UB	UB	UB	UB	UB
Max. Iteration	1000	1000	1000	1000	1000	1000	1000	1000	1000
Population Size	50	50	50	50	50	50	50	50	50
Mean Weight (kgf)	3200.15	3254.97	3129.03	3098.19	3166.31	3218.80	3075.87	3149.82	3108.81
Best Weight (kgf)	3056.36	3066.58	3097.14	3047.15	3078.32	3041.17	3067.88	3035.50	3047.98
Worst Weight (kgf)	3478.02	3745.91	3181.21	3141.01	3297.07	3692.74	3133.86	3320.91	3182.31
Std. Deviation	128.41	182.68	24.37	29.34	64.64	199.30	55.19	27.35	35.18
Saved Analyses (%)	65	49 / 0	65	58 / 0	54	58	59	64	57
Comp. Time (s)	108	153 / ---	189	206 / ---	---	---	---	---	---

* The algorithms are provided in Azad (2017).

68
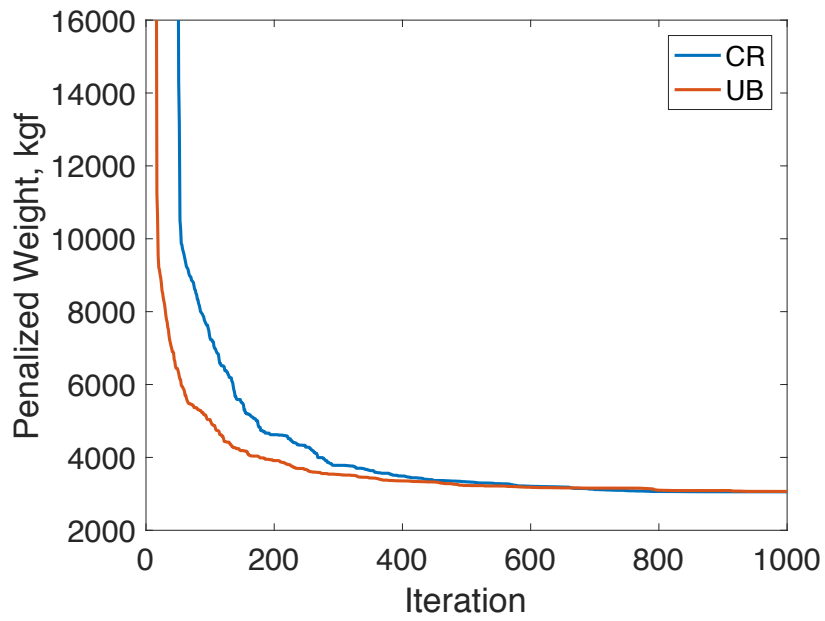
(a)
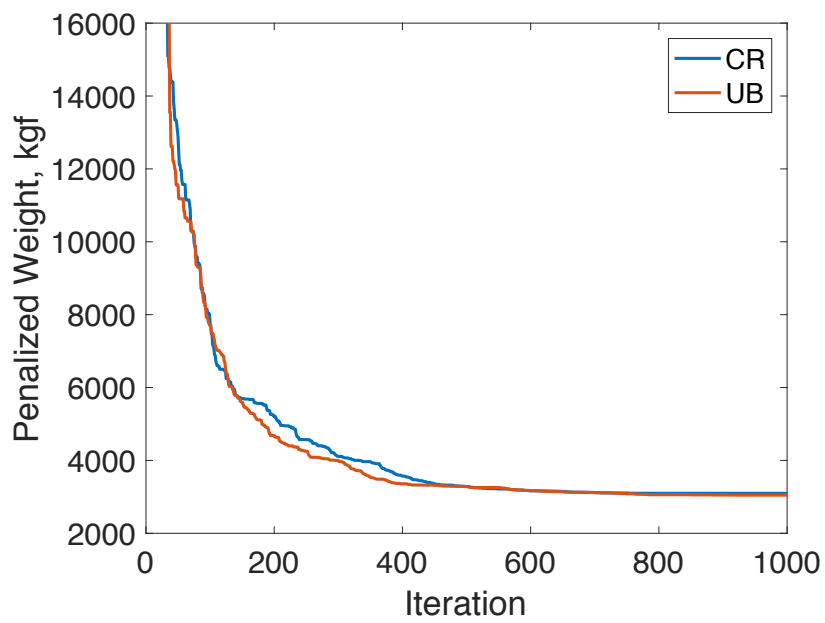
(b)

Figure 5.3. Convergence History of 117-Member Truss, (a) ADS (b) EBB
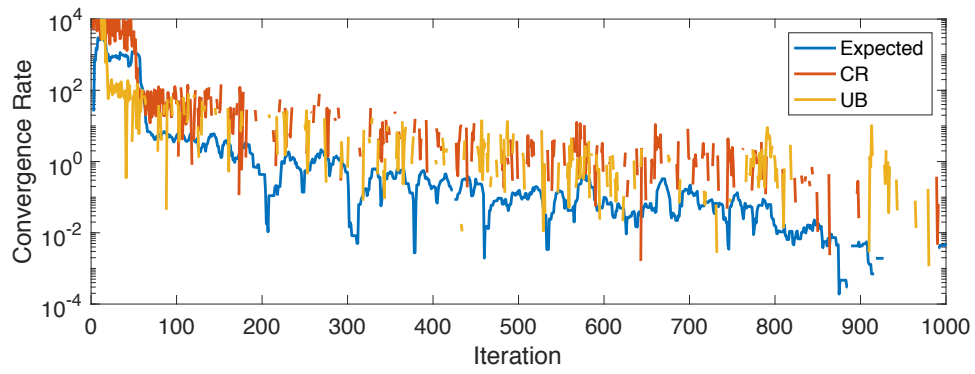
(a)
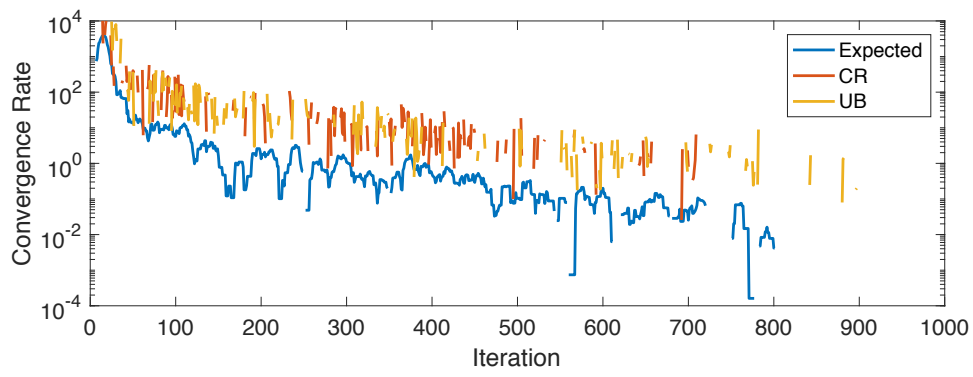
(b)

Figure 5.4. Convergence Rate Value in 117-Member Truss, (a) ADS (b) EBB

Figure 5.5. Structural Analyses Saving in 117-Member Truss, (a) ADS (b) EBB

71

5.3. 130-Bar Transmission Tower Example

The second problem is a steel transmission tower with 130 members and 33 joints as illustrated in Figure 5.6. The members are not grouped, and the optimization is carried out on each member of the truss, separately. The truss is loaded from five top nodes as illustrated in Table 5.3 and the self-weight of the structure is neglected. Additionally, displacement of the tower tip is restricted to 30 mm in x direction. The population size and maximum number of iterations are set to 50 and 1000, respectively.

Employing the EBB algorithm without any structural analyses saving strategies, Azad et al. (2014) acquired a design weight of 6059.5 kgf with a similar loading but using the LRFD-AISC (1994). In the present study, though, the ASD-AISC (1989) is employed for design of the trusses. According to Table 5.4, for the CR and UB approach integrated ADS algorithm, design weights of 7037.23 kgf and 7921.35 kgf are obtained, respectively. Furthermore, for the EBB version of the algorithms, design weights of 6919.38 kgf and 6972.91 kgf are obtained, respectively.

As denoted in the aforementioned table, Convergence Rate approach surpasses the Upper Bound approach in terms of the saved analyses. For instance, in ADS algorithm, the percentage of saved analyses is 68% for CR and 50% for UB approaches. Likewise, for the EBB algorithm, these values are equal to 65% for the CR and 56% for the UB approaches. An improvement in the computational time of the CR integrated metaheuristic algorithms, compared to the UB integrated methods, is visible, as well. For instance, the computational time of 146 s for the UB integrated ADS method is obtained; this value, however, is reduced to 101 s for the CR integrated ADS method. The same trend can also be noticed in CR and UB integrated EBB algorithms.

It is worth mentioning that nonetheless the intense disqualification of the individuals from entering the analyses procedure using the CR approach as

illustrated in Figure 5.8, no degradation in the quality of the optimum solution compared to the UB strategy is noticeable in Figure 5.7.

Table 5.3: Loading Cases of the 130-Member steel transmission tower

Node	X-Direction (kN)	Y-Direction (kN)	Z-Direction (kN)
29	100	0	0
30	100	0	0
31	0	25	0
32	0	25	0
33	0	0	-50
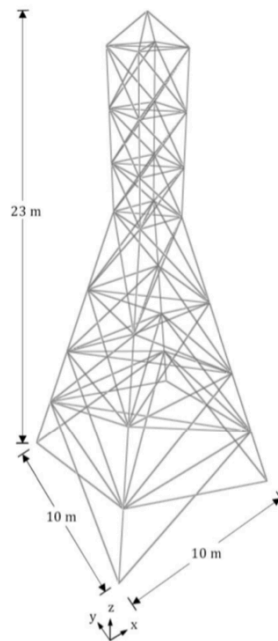
Figure 5.6. 130-Bar Transmission Tower, (Azad 2014)

Table 5.4: Optimum Design Results for 130-Member Transmission Tower

	ADS		EBB		PSO*	BB*	MBB*	EBB*	GSS*
	CR	UB/Std.	CR	UB/Std.	Std.	Std.	Std.	Std.	Std.
Max. Iteration	1000	1000	1000	1000	1000	1000	1000	1000	200
Population Size	50	50	50	50	50	50	50	50	1
Mean Weight (kgf)	7037.23	7921.35	6919.38	6972.91	6364.3	6742.9	6144.5	6059.5	6004.4
Best Weight (kgf)	6342.77	7127.63	6605.95	6569.95	6059.6	6427.8	5973.5	5853.9	5801.3
Worst Weight (kgf)	7925.49	9564.10	7386.84	7527.66	6611.4	7172.6	6434.7	6526.4	6118.5
Std. Deviation	437.92	806.40	275.35	309.67	227.3	303.8	188.9	240.4	87.6
Saved Analyses (%)	68	50 / 0	65	56 / 0	0	0	0	0	0
Comp. Time (s)	101	146 / ---	186	216 / ---	---	---	---	---	---

* The algorithms are provided in Azad et al. (2014).
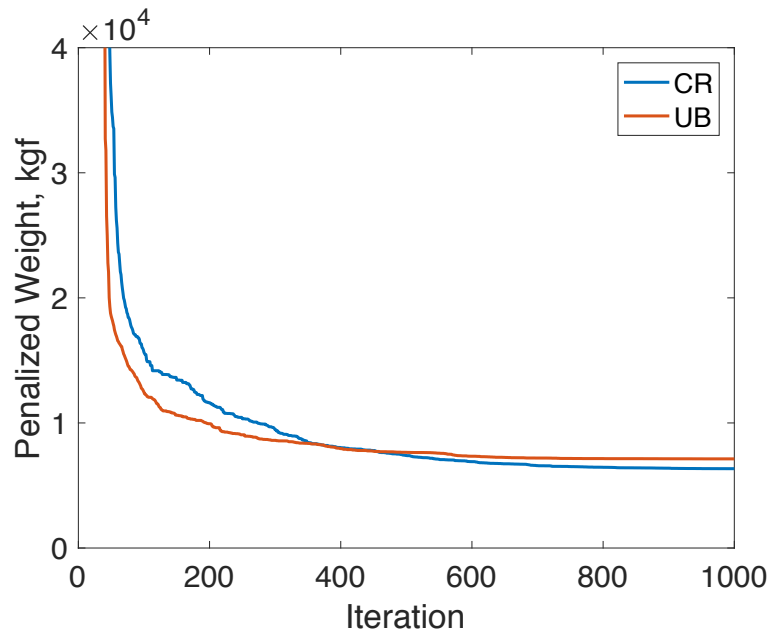
(a)
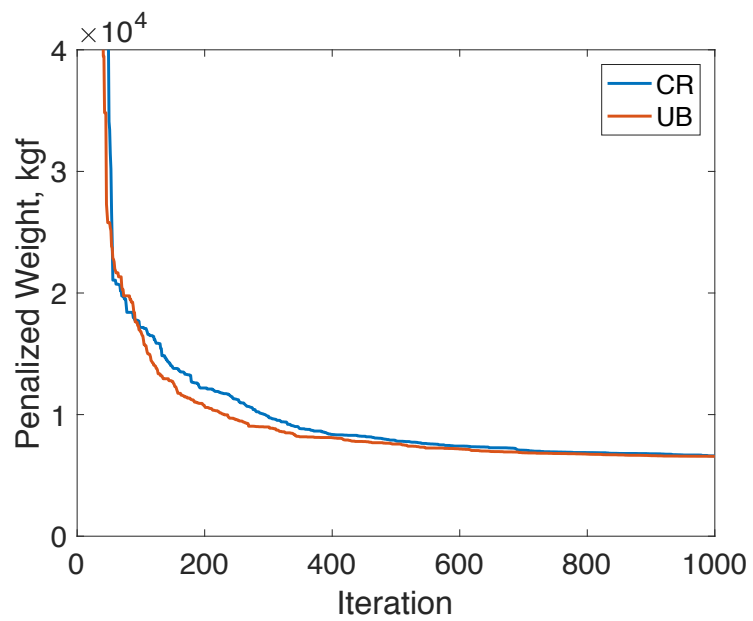
(b)

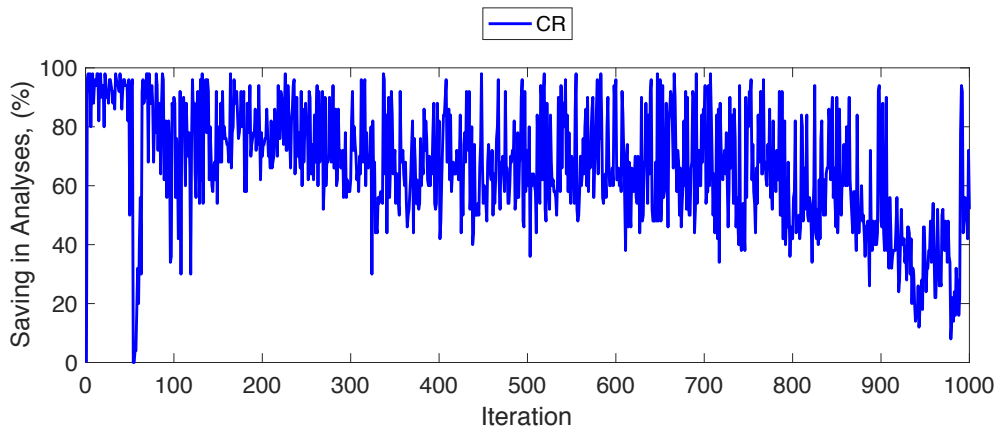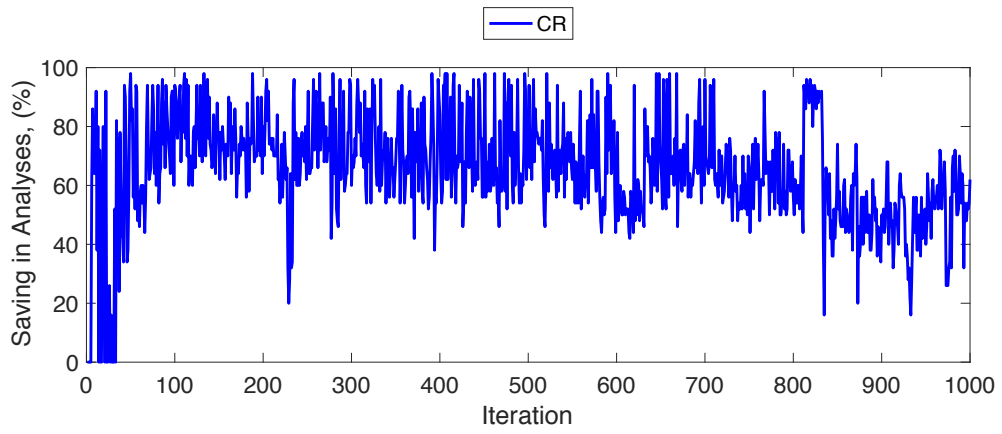Figure 5.7. Convergence History of 130-Member Tower, (a) ADS (b) EBB
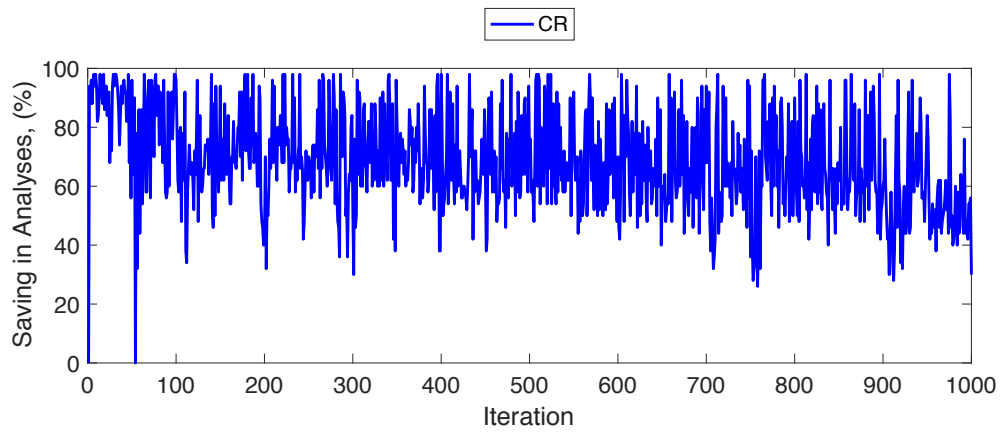
(a)
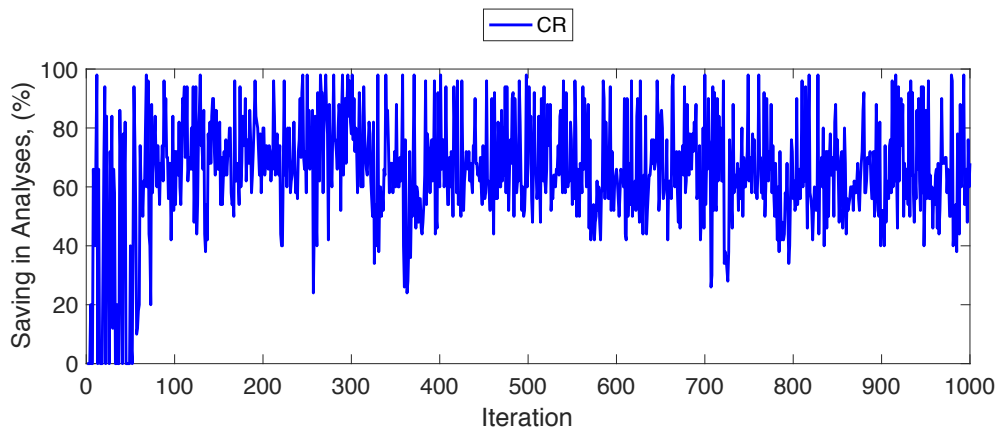
(b)

Figure 5.8. Structural Analyses Saving in 130-Member Tower, (a) ADS (b) EBB

5.4. 392-Bar Roof Truss Example

The third example is a steel roof truss as illustrated in Figure 5.9. The truss is composed of 392 members and 113 joints, and no grouping is carried out on the members. All top grid nodes are exposed to a single downward load of 15 kN. Moreover, vertical displacement of the central node of the bottom grid is restricted to 10 mm. The population size and maximum number of iterations are set to 50 and 2000, respectively.

Utilizing the EBB algorithm without any structural analyses saving strategies, Azad et al. (2014) have obtained a design weight of 2169.6 kgf in a similar loading condition as this study but using the LRFD-AISC (1994).

In the present study, however, the ASD-AISC (1989) is employed for design of the trusses. According to Table 5.5, design weights of 1964.93 kgf and 1851.49 kgf are obtained for the CR and UB approach integrated ADS algorithms, respectively. Furthermore, for the EBB version of the algorithm, design weights of 2054.75 kgf and 1992.43 kgf are obtained for the CR and UB approaches, respectively. As denoted in this table, CR surpasses the UB in saved analyses percentages in the ADS as well as the EBB algorithms. In ADS algorithm, the percentage of saved analyses is 79% for CR and 69% for UB methods. Likewise, for the EBB algorithm, these values are equal to 74% for the CR and 66% for the UB methods. Moreover, a significant decrease in the value of the computational time is also observed in CR integrated ADS and EBB algorithms compared to the UB integrated algorithms.

Table 5.5: Optimum Design Results for 392-Member Roof Truss

	ADS		EBB		PSO*	BB*	MBB*	EBB*	GSS*
	CR	UB/Std.	CR	UB/Std.	Std.	Std.	Std.	Std.	Std.
Max. Iteration	2000	2000	2000	2000	2000	2000	2000	2000	200
Population Size	50	50	50	50	50	50	50	50	1
Mean Weight (kgf)	1964.93	1851.49	2054.75	1992.43	3406.3	4013.1	2669.1	2169.6	2127.5
Best Weight (kgf)	1870.62	1761.94	1926.04	1913.70	3272.7	3645.1	2574.4	2116.3	2113.8
Worst Weight (kgf)	2109.88	1979.54	2298.63	2137.86	3603.1	4501.2	2775.9	2290.3	2146.9
Std. Deviation	80.60	70.00	105.92	73.80	159.7	376.5	83.3	81.5	9.6
Saved Analyses (%)	79	69 / 0	74	66 / 0	0	0	0	0	0
Comp. Time (s)	2367	3496 / ---	3046	4036 / ---	---	---	---	---	---

* The algorithms are provided in Azad et al. (2014).

78
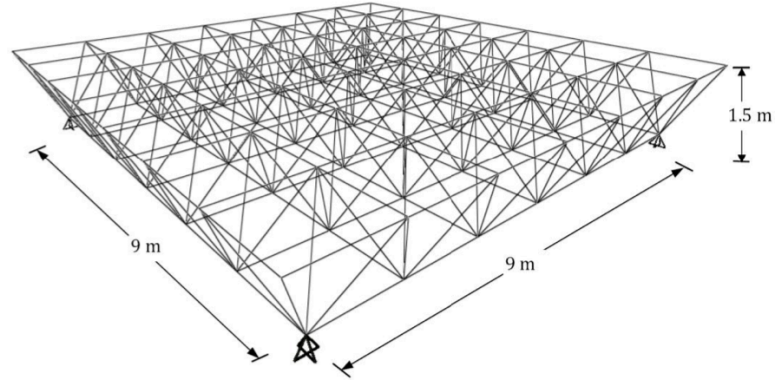
(a)
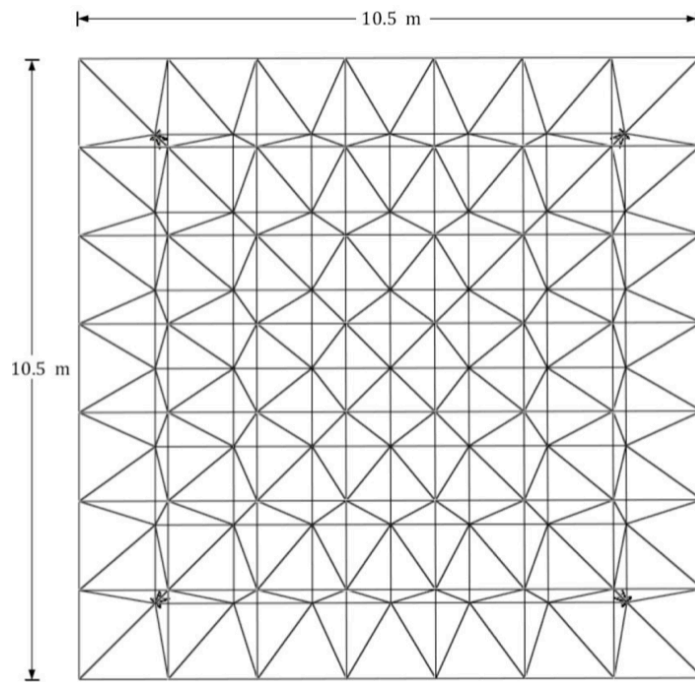
(b)

Figure 5.9. 392-Bar Roof Truss, (a) 3-D View (b) Top View (Azad et al. 2014)
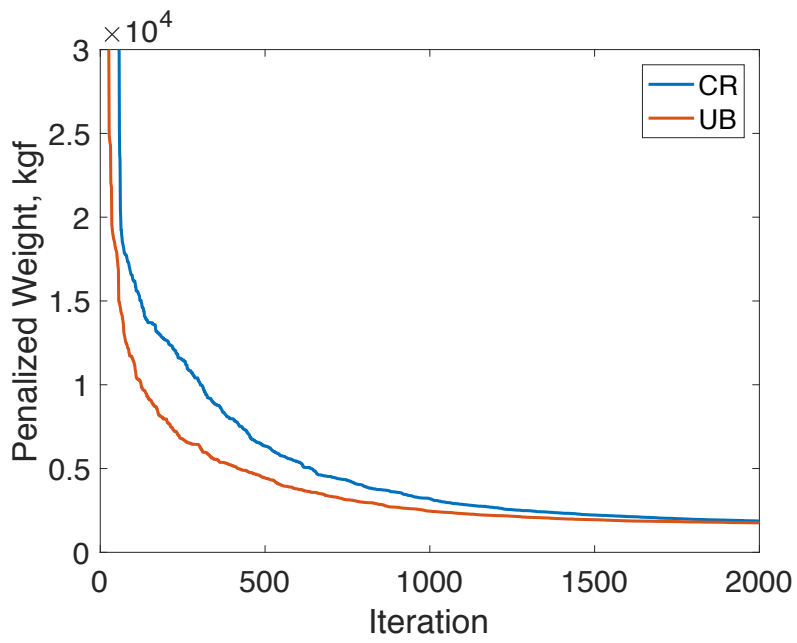
(a)
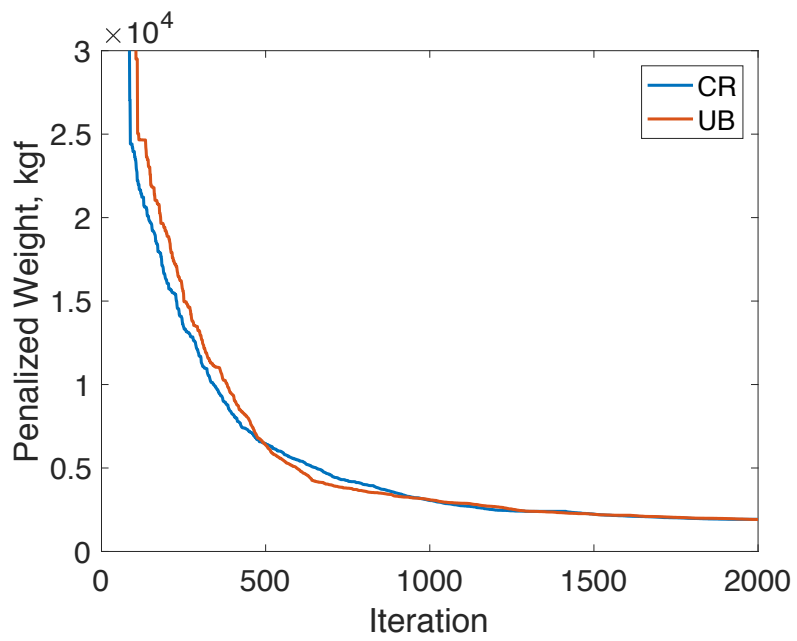
(b)

Figure 5.10: Convergence History of 392-Member Roof Truss, (a) ADS (b)
EBB
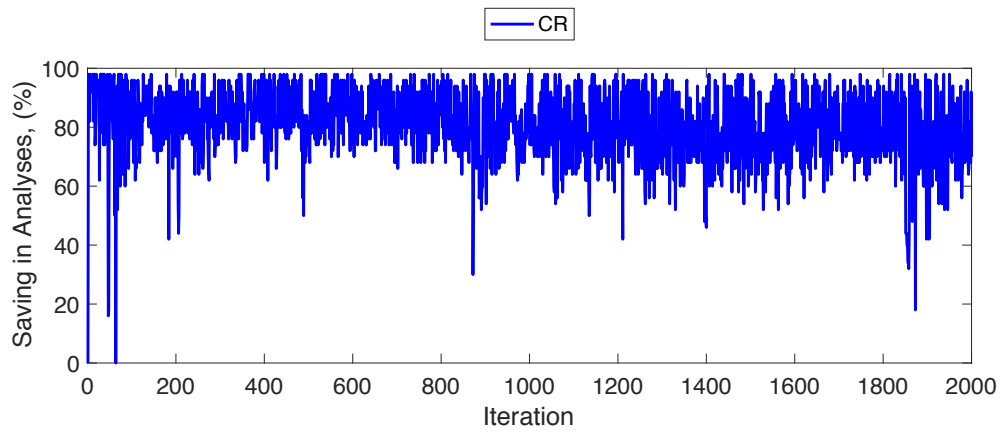
(a)
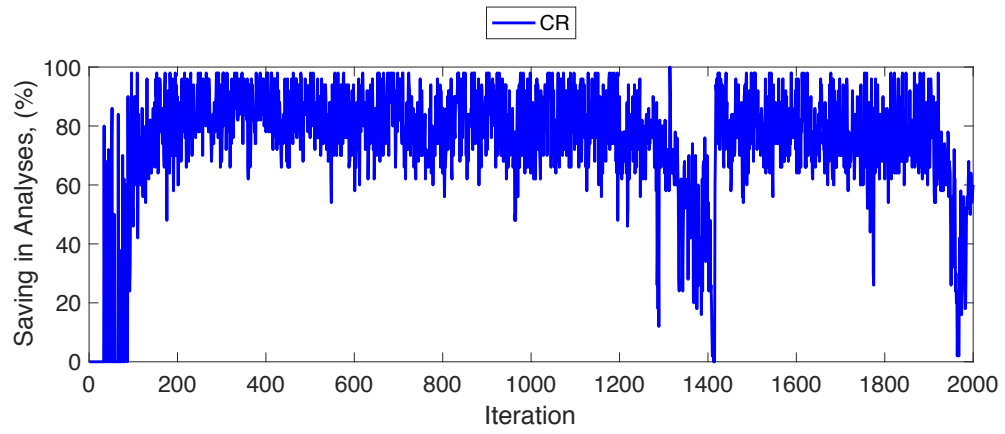
(b)

Figure 5.11. Structural Analyses Saving in 392-Member Truss, (a) ADS (b) EBB

5.5. Summary

Within the previous chapter, the Convergence Rate (CR) approach was proposed and merged into the previously defined Upper Bound (UB) method. Then, the new algorithm, was integrated into the ADS and EBB metaheuristic methods. With all these algorithms working in harmony, an improvement was observed in efficiency of the conventional ADS and EBB metaheuristic search algorithms.

Through this chapter, the new method is tested on three truss examples including the 117-bar cantilever truss, 130-bar transmission tower, and 394-bar double layer grid truss according to the ASD-AISC (1989). Based on the optimum design results, the CR approach integrated algorithms not only outperform the conventional UB algorithm in terms of the saved structural analyses percentages, but also maintains the accuracy and robustness of the original algorithm.

In conclusion, CR can be considered an effective way to lower the computational cost of the optimization process in large-scale structures without experiencing a degeneration in the quality of the outcomes. Thus, within the next section, optimum design of a large-scale onshore steel drilling rig structure with real-world loading cases and complex geometry will be carried out using the Convergence Rate integrated ADS and EBB algorithms.

CHAPTER 6

APPLICATION OF THE CONVERGENCE RATE INTEGRATED METAHEURISTIC SEARCH ALGORITHMS ON THE STEEL DRILLING RIG DESIGN

6.1. Introduction

Through this chapter, the structural model of a modular onshore drilling rig is optimized through the Convergence Rate integrated ADS and EBB metaheuristic search methods. For this purpose, the MATLAB computing environment based optimization code is linked to the SAP2000 v19.2.2 (2017) software through the Online Application Programming Interface (OAPI).

The structure is composed of 631 frames and 413 joints. For optimization purposes, however, the frames are grouped into 106 groups because of the practical issues in construction. The practical considerations include the symmetry of the structure as well as the continuous elements divided into some parts for analyses purposes. Furthermore, four types of sections are available as design variables including the European Wide Flange Beams, IPE Profiles, and Hollow Structural Sections (Circular and Square). The lists of the utilized structural sections are provided in Table 6.1 through Table 6.4.

6.2. Optimization Constraints

Two main constraints are considered while performing the optimization process. First, lateral displacement at the top of the mast tower is restricted to 50 cm. Moreover, the stress ratio values calculated through the Eqs. (3.11) to (3.14) are restricted to 0.95.

Table 6.1: European Wide Flange Beams, HE

HE							
100A	180A	240A	300A	340M	450M	600M	800M
100B	180B	240B	300B	360A	500A	650A	900A
120A	180M	240M	300C	360B	500B	650B	900B
120B	200A	260A	300M	360M	500M	650M	900M
140A	200B	260B	320A	400A	550A	700A	
140B	200M	260M	320B	400B	550B	700B	
160A	220A	280A	320M	400M	550M	700M	
160B	220B	280B	340A	450A	600A	800A	
160M	220M	280M	340B	450B	600B	800B	

Table 6.2: Hollow Structural Sections, Circular

TUBO-D							
101.6X3.6	127X4	152.4X4	193.7X4.5	273X5.6	355.6X6.3	419X7.1	82.5X3.2
108X3.6	133X4	159X4	219.1X5	298.5X5.9	368X6.3	457.2X7.1	88.9X3.2
114.3X3.6	139.7X4	168.3X4	244.5X5.4	323.9X5.9	406.4X6.3	76.1X3.2	82.5X3.2

Table 6.3: IPE Profiles, IPE

IPE							
100	180R	240O	330	400R	500R	600R	750x210
120	200	240R	330O	400V	500V	600V	750x222
140	200O	270	330R	450	550	750X137	
140R	200R	270O	360	450O	550O	750x147	
160	220	270R	360O	450R	550R	750x161	
160R	220O	300	360R	450V	550V	750x173	
180	220R	300O	400	500	600	750x185	
180O	240	300R	400O	500O	600O	750x196	

6.3. Optimization Results

The results of the optimization are according to Table 6.5. Using the Convergence Rate approach integrated ADS method, from the total optimum weight of 80.83 tonf, 36.52 tonf are for the Mast part and 44.32 tonf are for the substructure part. For EBB method, however, total weight is equal to 88.94 tonf, comprised of a 36.39 tonf mast as well as a 52.55 tonf substructure.

Table 6.4: Hollow Structural Sections, Square

TUBO					
100X100X10	140X140X22.2	180X180X35	240X240X16	280X280X25	340X340X22.2
100X100X12.5	140X140X25	200X200X12.5	240X240X17.5	280X280X28	340X340X25
100X100X14.2	140X140X7.1	200X200X14.2	240X240X20	280X280X30	340X340X28
100X100X16	140X140X8	200X200X16	240X240X22.2	280X280X35	340X340X30
100X100X17.5	160X160X10	200X200X17.5	240X240X25	280X280X40	340X340X35
100X100X5.4	160X160X12.5	200X200X20	240X240X28	300X300X16	340X340X40
100X100X5.9	160X160X14.2	200X200X22.2	240X240X30	300X300X17.5	360X360X20
100X100X7.1	160X160X16	200X200X25	240X240X35	300X300X20	360X360X22.2
100X100X8	160X160X17.5	200X200X28	240X240X40	300X300X22.2	360X360X25
120X120X10	160X160X20	200X200X30	260X260X14.2	300X300X25	360X360X28
120X120X12.5	160X160X22.2	200X200X35	260X260X16	300X300X28	360X360X30
120X120X14.2	160X160X25	220X220X12.5	260X260X17.5	300X300X30	360X360X35
120X120X16	160X160X28	220X220X14.2	260X260X20	300X300X35	360X360X40
120X120X17.5	160X160X30	220X220X16	260X260X22.2	300X300X40	380X380X20
120X120X20	180X180X10	220X220X17.5	260X260X25	320X320X17.5	380X380X22.2
120X120X22.2	180X180X12.5	220X220X20	260X260X28	320X320X20	380X380X25
120X120X7.1	180X180X14.2	220X220X22.2	260X260X30	320X320X22.2	380X380X28
120X120X8	180X180X16	220X220X25	260X260X35	320X320X25	380X380X30
140X140X10	180X180X17.5	220X220X28	260X260X40	320X320X28	380X380X35
140X140X12.5	180X180X20	220X220X30	280X280X14.2	320X320X30	380X380X40
140X140X14.2	180X180X22.2	220X220X35	280X280X16	320X320X35	400X400X22.2
140X140X16	180X180X25	220X220X40	280X280X17.5	320X320X40	400X400X25
140X140X17.5	180X180X28	240X240X12.5	280X280X20	340X340X17.5	400X400X28
140X140X20	180X180X30	240X240X14.2	280X280X22.2	340X340X20	400X400X30

Table 6.5: Onshore Drilling Rig Optimization Results

	ADS	EBB
Max. Iterations	500	500
Population Size	50	50
Total Weight (tonf)	80.83	88.94
Saved Analyses (%)	90.46	91.75
Number of Analyses	2385	2063
Computational Time (s)	76191	79697

(a)   (b)
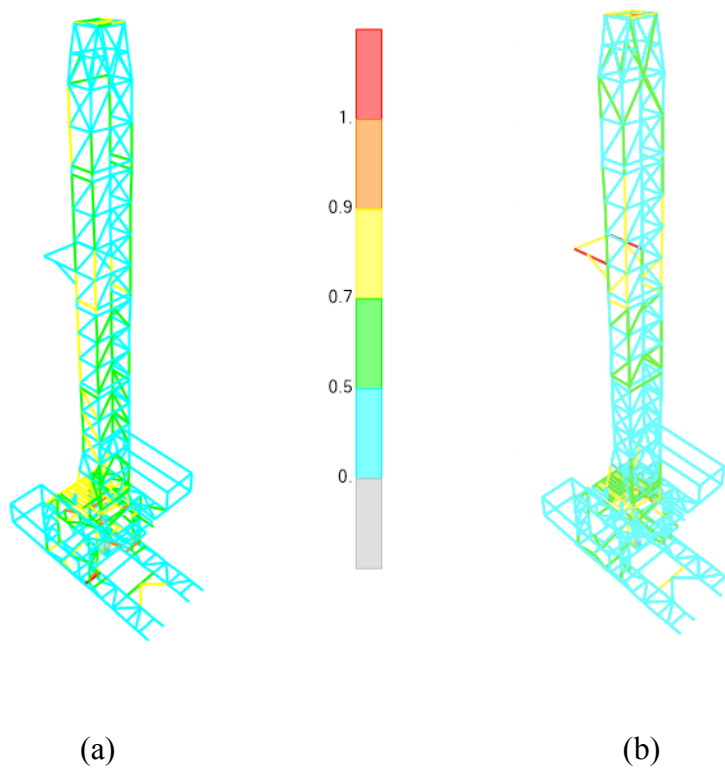
Figure 6.1. Land Rig Design Results, (a) ADS (b) EBB
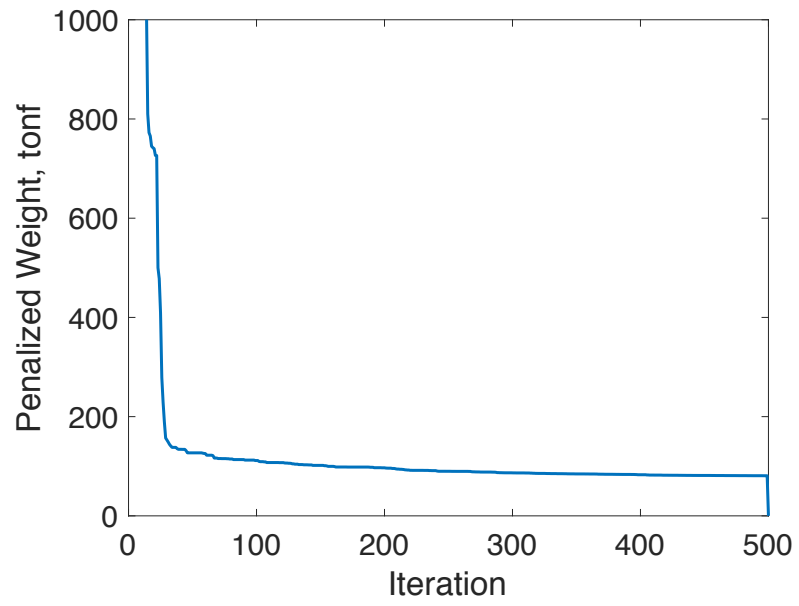
(a)
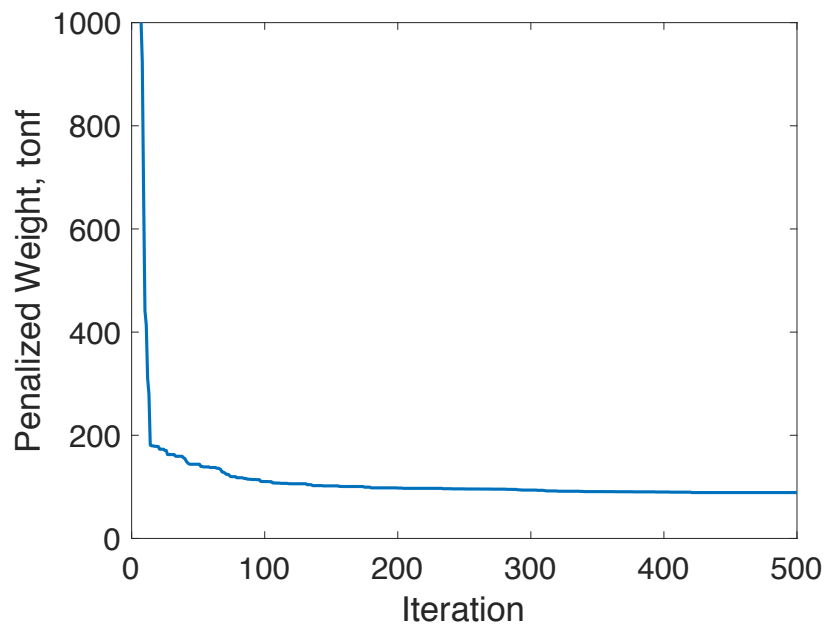
(b)

Figure 6.2. Convergence History of the Onshore Drilling Rig, (a) ADS (b) EBB
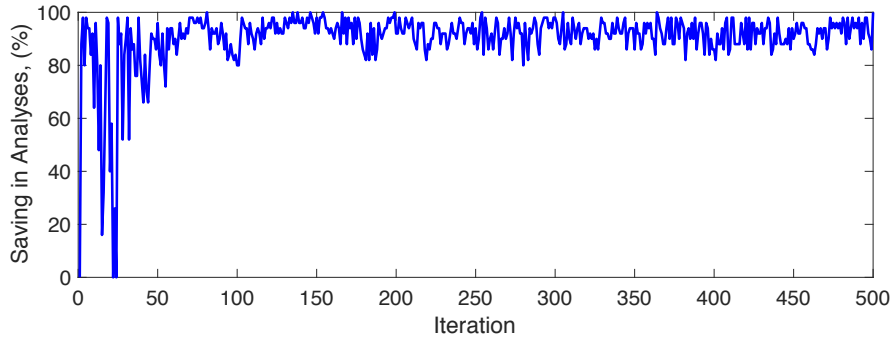
(a)
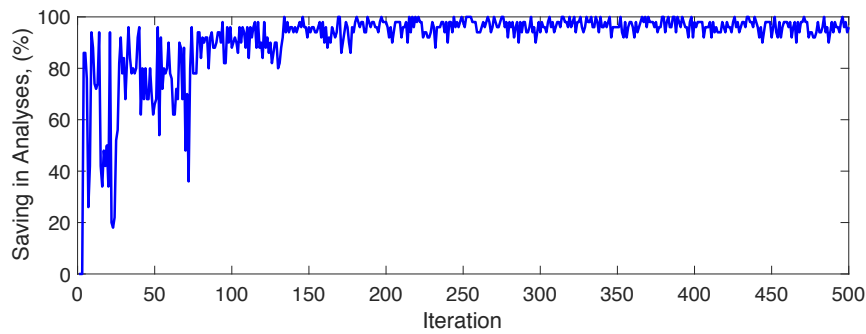
(b)

Figure 6.3. Onshore Drilling Rig Structural Analyses Savings, (a) ADS (b) EBB

Based on the Figure 6.2, it is clear that the integrated version of the ADS algorithm and CR approach has been able to locate the optimum weight of the land rig in 500 iterations, since after 300 iterations no significant improvement in the quality of the optimum solution can be observed. This also applies to the EBB version of the code. Moreover, taking the 50 individuals within a population into consideration, without using the CR strategy, the algorithm had to perform 25000 structural analyses in order to locate the solution. This number is easily obtained by multiplying the number of iterations by the number of individuals within a population. Using the CR strategy, however, decreases the required number of structural analyses by approximately 91% for the ADS and EBB algorithms. In other words, 22500 individuals are disqualified from being analyzed and less than 2500 structural

analyses are performed by the algorithm. This vast amount of efficiency is obtained by integrating a simple, yet efficient, code into the main algorithm without any significant expenses. The structural sections obtained for the onshore drilling rig are outlined in Table 6.6.

Table 6.6: Optimum Designs Obtained for Onshore Drilling Rig

Group	Section Name, ADS	Section Name, EBB
1	IPE400	IPE400
2	IPE400	IPE400
3	HE200B	HE240A
4	HE100B	HE200A
5	IPE400	IPE400
6	IPE400	IPE400
7	TUBO100X100X5.4	TUBO140X140X8
8	TUBO100X100X10	TUBO120X120X8
9	TUBO100X100X5.4	TUBO100X100X5.9
10	TUBO100X100X5.4	TUBO100X100X5.4
11	TUBO240X240X12.5	TUBO120X120X8
12	TUBO120X120X7.1	TUBO280X280X17.5
13	TUBO140X140X7.1	TUBO240X240X12.5
14	TUBO140X140X7.1	TUBO120X120X8
15	TUBO180X180X10	TUBO180X180X10
16	TUBO100X100X5.4	TUBO120X120X8
17	TUBO180X180X10	TUBO300X300X25

Table 6.6 (Continued)

Group	Section Name, ADS	Section Name, EBB
18	TUBO100X100X5.4	TUBO100X100X10
19	TUBO100X100X5.4	TUBO100X100X5.4
20	TUBO280X280X14.2	TUBO100X100X8
21	TUBO280X280X14.2	TUBO100X100X7.1
22	TUBO140X140X7.1	TUBO100X100X7.1
23	TUBO140X140X7.1	TUBO100X100X16
24	TUBO120X120X7.1	TUBO100X100X10
25	TUBO280X280X14.2	TUBO240X240X17.5
26	TUBO300X300X16	TUBO300X300X16
27	TUBO120X120X7.1	TUBO120X120X10
28	TUBO180X180X22.2	TUBO240X240X12.5
29	TUBO220X220X12.5	TUBO180X180X16
30	TUBO180X180X16	TUBO280X280X14.2
31	TUBO160X160X12.5	TUBO140X140X14.2
32	TUBO220X220X12.5	TUBO220X220X14.2
33	TUBO180X180X10	TUBO140X140X17.5
34	TUBO220X220X12.5	TUBO260X260X14.2
35	HE450A	HE600A
36	HE160A	HE120A
37	HE180A	HE100B
38	HE120A	HE120B
39	HE100A	HE160A
40	HE140A	HE120A
41	HE120A	HE400A
42	HE240A	HE320A
43	HE180A	HE120A

Table 6.6 (Continued)

Group	Section Name, ADS	Section Name, EBB
44	HE200A	HE180A
45	HE160A	HE200B
46	HE100A	HE260A
47	HE140A	HE280A
48	HE180A	HE180A
49	HE180A	HE180A
50	HE360A	HE400A
51	TUBO-D457.2X7.1	TUBO-D457.2X7.1
52	HE100A	HE400A
53	HE120A	HE320A
54	HE180A	HE180A
55	HE140A	HE220A
56	HE100A	HE180B
57	HE120B	HE240B
58	HE220A	HE300A
59	HE180A	HE100A
60	HE120A	HE180B
61	HE320A	HE300A
62	HE140B	HE400A
63	IPE750X137	IPE600
64	HE120B	HE400A
65	IPE750x173	IPE750X137
66	IPE750X137	IPE750x161
67	IPE750X137	IPE750X137
68	HE160A	HE240A
69	HE280A	HE100A

Table 6.6 (Continued)

Group	Section Name, ADS	Section Name, EBB
70	HE100A	HE100A
71	IPE750x222	IPE750x196
72	HE100A	HE100A
73	HE140A	HE220A
74	HE140A	HE220A
75	HE600A	HE500A
76	IPE750x147	IPE500
77	HE600A	HE800A
78	HE900A	HE550A
79	HE800B	HE650A
80	HE900A	HE900B
81	HE550A	HE900B
82	HE320B	HE340B
83	HE400A	HE400A
84	HE100A	HE320A
85	HE120B	HE100A
86	HE280A	HE200A
87	IPE100	IPE750x185
88	HE700A	HE550B
89	HE100A	HE240A
90	HE400A	HE400B
91	IPE330	IPE360
92	HE500A	HE500A
93	HE240A	HE140A
94	HE100A	HE180A
95	HE100A	HE120A

Table 6.6 (Continued)

Group	Section Name, ADS	Section Name, EBB
96	HE180A	HE360A
97	HE120A	HE300A
98	HE100A	HE200A
99	HE140A	HE340B
100	HE240B	HE280B
101	HE400A	HE550A
102	TUBO-D273X5.6	TUBO-D273X5.6
103	TUBO220X220X12.5	TUBO220X220X12.5
104	TUBO260X260X14.2	TUBO340X340X28
105	TUBO280X280X20	TUBO300X300X17.5
106	TUBO240X240X12.5	TUBO260X260X14.2

6.3.1. Displacements

Displacement values at the top of the tower designed by the CR approach integrated ADS method are illustrated in Table 6.7. It is apparent that the displacement values at any case falls below the limit value of 50 cm. Moreover, in normal operational environment, which is the dominant and most likely condition during the lifetime of the land rig, displacement values are even lower than 35 cm, providing a safe working environment for the personnel.

6.3.2. Base Shear, Wind Load

Wind loads imposed upon the structure designed by the CR approach integrated ADS method are provided in Table 6.8. Two load cases for wind loads are defined such that the first load case is the wind load imposed upon the structural elements as well as the two cabins in both sides of the drilling floor. These wind absorbing

elements and walls are present in every drilling stage and therefore, are considered in all load combinations that take the wind loads into consideration. The second wind load case is the case associated with the wind load absorbed by the drilling pipes while stored on the setback area. Since this is a temporary situation and the pipes stored on the setback can be lowered any time, this wind load case is only present in load combinations having the setback load as one of the main load cases.

6.3.3. Participating Mass

As illustrated in Table 6.9, for mass scenarios 1 and 2, the 90% mass participation is attained within the initial 8 modes. Moreover, according to Table 6.10, for mass scenario 1 and 2, the natural periods of 2.95 and 3.21 seconds are obtained for the tower designed by the CR approach integrated ADS method. It is worth mentioning that these two scenarios are only different in the position of the travelling equipment such that as denoted in Table 2.14, in mass scenario 1 the travelling equipment is at the lowest position, while in mass scenario 2 it is located at the highest possible position, i.e. top part of the mast. Thus, in the second scenario, an increase in the natural period of the structure can be perceived. Moreover, despite the presence of the hook load in load combinations associated with the second mass scenario, since most of the drilling pipes are below the earth's surface and do not contribute to the mass of the structure, no major difference in the natural periods of the two scenarios are observed.

Likewise, for mass scenarios 3 and 4, the required 90% mass participation ratios are acquired in the initial 11 and 10 modes, respectively. Furthermore, based on Table 6.10, the natural periods of these scenarios are equal to 5.01 and 4.57 seconds, respectively. This is quite expectable since the mass scenario 3 takes the full setback loading into consideration and consequently, due to the major increase in the participating mass of the structure, a high natural period is obtained. However, in mass scenario 4, since only 75% of the rated setback load as well as 50% of the rated static hook load are applied upon the structure, a decrease in the value of the natural period of the steel structure is observable. This is due to the reduction in the

participating mass of the setback load as well as the negligible participation mass of the hook load.

Table 6.7: Top Point Displacement, ADS

Combo	Load Case		Ux (cm)	Uy (cm)	Load Case		Ux (cm)	Uy (cm)
1a	Temp +50, Wind	X+	3.89	-13.55	Temp -30, Wind	X+	3.89	-14.21
		X-	-13.93	-13.55		X-	-13.93	-14.21
		Y+	-5.02	-5.60		Y+	-5.02	-6.27
		Y-	-5.02	-21.49		Y-	-5.02	-22.15
1b		X+	8.85	10.97		X+	8.85	10.30
		X-	-8.98	10.97		X-	-8.98	10.30
		Y+	-0.06	18.91		Y+	-0.06	18.24
		Y-	-0.06	3.02		Y-	-0.06	2.36
2		X+	28.09	2.86		X+	28.09	2.20
		X-	-28.22	2.86		X-	-28.22	2.20
		Y+	-0.06	33.46		Y+	-0.06	32.80
		Y-	-0.06	-27.74		Y-	-0.06	-28.40
3a		X+	27.23	10.97		X+	27.23	10.30
		X-	-27.36	10.97		X-	-27.36	10.30
		Y+	-0.06	35.29		Y+	-0.06	34.62
		Y-	-0.06	-13.35		Y-	-0.06	-14.02

Table 6.7 (Continued)

Combo		Load Case	Ux (cm)	Uy (cm)	Load Case	Ux (cm)	Uy (cm)
3b-Bare		X (Max)	23.38	6.84	X (Max)	23.38	6.17
		X (Min)	-23.50	-10.65	X (Min)	-23.50	-11.31
		Y (Max)	7.31	26.07	Y (Max)	7.31	25.41
		Y (Min)	-7.44	-29.88	Y (Min)	-7.44	-30.55
3b-Hook		X (Max)	21.11	-8.23	X (Max)	21.11	-8.90
		X (Min)	-29.16	-27.17	X (Min)	-29.16	-27.84
		Y (Max)	3.92	12.51	Y (Max)	3.92	11.84
		Y (Min)	-11.98	-47.91	Y (Min)	-11.98	-48.57
3b-Rotary	Temp +50, EQ	X (Max)	25.07	11.38	X (Max)	25.07	10.72
		X (Min)	-25.20	-7.56	X (Min)	-25.20	-8.23
		Y (Max)	7.88	32.12	Y (Max)	7.88	31.45
		Y (Min)	-8.01	-28.30	Y (Min)	-8.01	-28.96
3b-Setback		X (Max)	35.92	19.38	X (Max)	35.92	18.71
		X (Min)	-36.05	-6.98	X (Min)	-36.05	-7.65
		Y (Max)	10.75	50.01	Y (Max)	10.75	49.34
		Y (Min)	-10.88	-37.61	Y (Min)	-10.88	-38.28
3b-Hook-Setback		X (Max)	31.32	6.52	X (Max)	31.32	5.85
	Temp -30, EQ	X (Min)	-36.40	-17.92	X (Min)	-36.40	-18.59
		Y (Max)	7.65	34.85	Y (Max)	7.65	34.18
		Y (Min)	-12.73	-46.25	Y (Min)	-12.73	-46.91
3b-Rotary-Setback		X (Max)	33.79	18.78	X (Max)	33.79	18.11
		X (Min)	-33.92	-5.66	X (Min)	-33.92	-6.33
		Y (Max)	10.13	47.10	Y (Max)	10.13	46.44
		Y (Min)	-10.26	-33.99	Y (Min)	-10.26	-34.66

Table 6.8: Base Reaction (Wind Loads), ADS

Load Case	Fx (tonf)	Fy (tonf)	Mx (tonf-cm)	My (tonf-cm)	Mz (tonf-cm)
WIND40-X	9.59	0.00	0.00	16739.68	400.50
WIND40-Y	0.00	6.77	14894.50	0.00	0.00
WIND70-X	29.36	0.00	0.00	51265.26	1226.53
WIND70-Y	0.00	20.73	45614.42	0.00	0.00
WIND95-X	54.08	0.00	0.00	94422.24	2259.06
WIND95-Y	0.00	38.17	84014.31	0.00	0.00
WIND40-X-Pipes	3.42	0.00	0.00	7940.17	872.38
WIND40-Y-Pipes	0.00	3.33	7736.58	0.00	0.00
WIND70-X-Pipes	10.48	0.00	0.00	24316.77	2671.65
WIND70-Y-Pipes	0.00	10.21	23693.27	0.00	0.00

6.3.4. Global Buckling

Global buckling factors of the onshore drilling rig designed by the CR approach integrated ADS method are illustrated in Table 6.11. This factor denotes the required increase in the value of the applied load which will result in the global buckling of the structure. For the first mode, if the value of the loads imposed upon the structure is increased by 2.65 time, a global buckling will occur.

Table 6.9: Cumulative Mass Participation, ADS

Mass	Cumulative Mass Participation		Mass	Cumulative Mass Participation	
	Mode No. (X)	Mode No. (Y)		Mode No. (X)	Mode No. (Y)
Mass Source 1	90% Mass Participation		Mass Source 2	90% Mass Participation	
	7	8		7	8
	100% Mass Participation			100% Mass Participation	
	150	150		150	150
Mass Source 3	90% Mass Participation		Mass Source 4	90% Mass Participation	
	11	10		7	10
	100% Mass Participation			100% Mass Participation	
	150	150		150	150
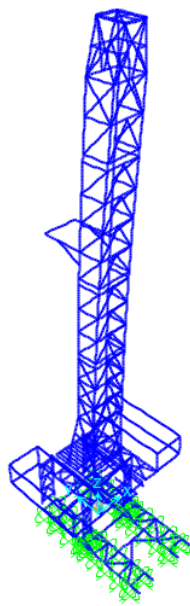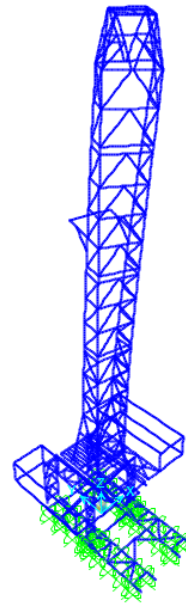
(a)   (b)

Figure 6.4. Modes Shapes for the First Mass Scenario (a) 1st Mode (b) 2nd Mode

Table 6.10: Periods for Various Mode Shapes, ADS

Mass	Mode No.	Period (s)	Mass Participation Ratio		Mass	Mode No.	Period (s)	Mass Participation Ratio	
			Ux	Uy				Ux	Uy
Participating Mass 1	1	2.957	0.0183	0.3660	Participating Mass 2	1	3.211	0.0205	0.4064
	2	2.870	0.3393	0.0204		2	3.113	0.3738	0.0229
	3	0.949	0.0664	0.0000		3	1.009	0.0678	0.0000
	4	0.597	0.2724	0.0004		4	0.601	0.2089	0.0004
	5	0.481	0.0063	0.3352		5	0.475	0.0005	0.0954
	6	0.468	0.0016	0.1375		6	0.461	0.0045	0.3231
Participating Mass 3	1	5.005	0.4441	0.0001	Participating Mass 4	1	4.574	0.4359	0.0002
	2	3.658	0.0001	0.4408		2	3.547	0.0003	0.4352
	3	1.632	0.0205	0.0000		3	1.572	0.0203	0.0000
	4	0.948	0.1603	0.0008		4	0.907	0.1488	0.0005
	5	0.822	0.2078	0.0001		5	0.754	0.2089	0.0006
	6	0.784	0.0006	0.2991		6	0.725	0.0011	0.3081

Table 6.11: Global Buckling Factors, ADS

Mode No.	Buckling Factor, X	Buckling Factor, Y
1	2.6556	2.7472
2	2.8646	2.8368
3	7.4707	6.8950
4	8.0419	8.4026

6.3.5. Base Shear, Seismic Load

Base shear of the onshore drilling rig designed by the CR approach integrated ADS method due to the seismic loads are provided in Table 6.12. A comparison of the seismic loads determined through the RSA as well as the ELFP methods illustrates that the initial method gives higher based shear values and thus, the requirements of the Section 2.8.5 of the Turkish Seismic Code (2007) do not govern.

Table 6.12: Base Reaction (Seismic Loads), ADS

Mass	Load Case		Fx (tonf)	Fy (tonf)	Fz (tonf)	TSC Check
Mass Source 1	RSA	X	39.65	14.91	0.90	OK
		Y	12.24	48.75	2.88	OK
	ELFP	X	28.15	8.45	0.00	OK
		Y	8.45	28.15	0.00	OK
Mass Source 2	RSA	X	37.31	13.70	0.94	OK
		Y	11.52	44.73	3.01	OK
	ELFP	X	26.65	8.00	0.00	OK
		Y	8.00	26.65	0.00	OK
Mass Source 3	RSA	X	52.98	20.10	7.06	OK
		Y	16.08	66.51	23.32	OK
	ELFP	X	36.21	10.86	0.00	OK
		Y	10.86	36.21	0.00	OK
Mass Source 4	RSA	X	48.75	18.23	6.62	OK
		Y	14.81	60.26	21.78	OK
	ELFP	X	34.57	10.37	0.00	OK
		Y	10.37	34.57	0.00	OK

6.3.6. Base Shear, Design Load Combinations

Base shear values of the land rig due to the load combinations 1 to 3 are given in Table 6.13.

Table 6.13: Base Reactions (Design Load Combinations), ADS

Combo	Load Case	Fx (tonf)	Fy (tonf)	Fz (tonf)
1a	Wind X+	-12.52	7.06	943.77
	Wind X-	13.50	7.06	943.77
	Wind Y+	0.49	-3.04	943.51
	Wind Y-	0.49	17.16	944.02
1b	Wind X+	-14.52	-2.29	874.46
	Wind X-	11.50	-2.29	874.46
	Wind Y+	-1.51	-12.39	874.20
	Wind Y-	-1.51	7.81	874.72
2	Wind X+	-55.59	-2.29	618.46
	Wind X-	52.57	-2.29	618.46
	Wind Y+	-1.51	-40.46	617.01
	Wind Y-	-1.51	35.89	619.91
3a	Wind X+	-41.35	-2.29	874.46
	Wind X-	38.33	-2.29	874.46
	Wind Y+	-1.51	-33.22	873.67
	Wind Y-	-1.51	28.65	875.25

Table 6.13 (Continued)

Combo	Load Case, EQ		Fx (tonf)	Fy (tonf)	Fz (tonf)
3b	Bare	X (Max)	38.14	12.62	269.39
		X (Min)	-41.16	-17.20	267.60
		Y (Max)	10.73	46.46	271.38
		Y (Min)	-13.75	-51.04	265.61
	Hook	X (Max)	37.40	18.89	604.85
		X (Min)	-37.22	-8.50	602.97
		Y (Max)	11.61	49.92	606.92
		Y (Min)	-11.43	-39.54	600.90
	Rotary	X (Max)	35.80	11.41	549.41
		X (Min)	-38.82	-15.98	547.53
		Y (Max)	10.01	42.44	551.48
		Y (Min)	-13.03	-47.02	545.46
3b	Setback	X (Max)	51.47	17.81	531.56
		X (Min)	-54.49	-22.39	517.43
		Y (Max)	14.57	64.22	547.82
		Y (Min)	-17.59	-68.80	501.17
	Hook-Setback	X (Max)	48.24	20.61	676.75
		X (Min)	-49.26	-15.84	663.51
		Y (Max)	14.30	62.65	691.91
		Y (Min)	-15.32	-57.88	648.35
	Rotary-Setback	X (Max)	47.24	15.94	642.10
		X (Min)	-50.26	-20.52	628.86
		Y (Max)	13.30	57.98	657.26
		Y (Min)	-16.32	-62.55	613.70

CHAPTER 7

CONCLUSION

7.1. Concluding Remarks

In the present study, an efficient method for optimization of the large-scale steel structures is developed. Two main purposes are sought from the application of this approach. First, improving the efficiency of the metaheuristics in dealing with the large-scale structural engineering problems; second, application of the developed code for the optimum design of a large-scale onshore drilling rig.

Subsequent to a concise introduction of the traditional, as well as the modern optimization methods within the first chapter, provisions governing the analyses and design of the onshore drilling rigs are provided through the second chapter. Afterwards, since these drilling rigs are designed using the ASD-AISC (1989) standard, strength and serviceability requirements of the steel trusses and frames according to the above mentioned standard are outlined within the third chapter. Through chapter 4, a succinct review of the recent attempts in reducing the required computational efforts in optimization of the large-scale steel structures is provided. Then, a new strategy named the Convergence Rate approach for increasing the efficiency of the metaheuristic methods is outlined. This strategy is based on the calculation of the expected value of the objective function for the succeeding iterations. Thus, if the objective function value of an individual within the next iteration is less than the expected value, the optimization is brought to a halt and the rest of the candidates within that population are not analyzed. Later on, a brief explanation of the Upper Bound strategy is provided and then, a hybridized version of the Convergence Rate and Upper Bound methods is introduced and integrated

into two well-established optimization methods named asa the Adaptive Dimensional Search method and Exponential Big Bang-Big Crunch method.

Optimization of three benchmark steel truss problems according to the ASD-AISC (1989) standard within the fifth chapter ascertains the efficiency and applicability of the proposed method both in reducing the required computational effort and time, as well as in maintaining the quality of the objective function. Moreover, the results from the literature, which are also illustrated within this chapter, demonstrate the efficiency of the algorithm.

Through Chapter 6, though, optimum design of an onshore drilling rig is carried out using the newly proposed Convergence Rate approach integrated metaheuristic algorithms. While the real loading scenarios are applied upon the structure, design of the drilling rig is carried out according to the aforementioned standards. It has been shown that in spite of the 90% reduction in the number of the performed structural analyses, the proposed algorithm was still able to locate an acceptable optimum weight for the structure. This amount of the structural analyses reduction is significant and clearly satisfies the purposes of the theses. In fact, copious number of structural analyses is considered a drawback in the optimization of the real-world structural problems, since each structural analysis takes a considerable amount of time. The required time to perform 2385 analyses in CR integrated ADS method is 21.16 hours, while for the CR integrated EBB method, the required time for performing 2063 structural analyses is about 22.14 hours. Therefore, the newly proposed algorithm can be an efficient solution in tackling the aforementioned shortcoming of the metaheuristics.

7.2. Future Research

In Chapter 6, size optimization of an onshore drilling rig structure was performed through the Convergence Rate approach integrated into the ADS and EBB algorithms. Including the topology optimization algorithm can also be fruitful in design of the land rigs. Moreover, the proposed computationally efficient optimization method can be utilized for optimum design of offshore drilling rigs

having different load cases and steel materials, as well. Moreover, some improvements can be carried out on the analytical model for the precise analysis of the land rig structure, such as including the time history domain analyses method for the seismic load calculation, as well as including the spring restraints instead of the pins for the exact modelling of the soil-structure interaction.

REFERENCES

Adeli, H., & Kamal, O. (1986). Efficient optimization of space trusses. Computers & Structures, 24(3), 501–511.

Ahrari, A., Atai, A. A., & Deb, K. (2015). Simultaneous topology, shape and size optimization of truss structures by fully stressed design based on evolution strategy. Engineering Optimization, 47(8), 1063–1084.

Alatas, B. (2011). Uniform Big Bang-Chaotic Big Crunch optimization. Communications in Nonlinear Science and Numerical Simulation, 16, 3696–3703.

API Recommended Practice 9B. (2005). Application, Care, and Use of Wire Rope for Oil Field Service. American Petroleum Institute.

API RP 2A-WSD. (2014). Recommended Practice for Planning, Designing, and Constructing Fixed Offshore Platforms. American Petroleum Institute.

API Specification 4F. (2013). Specification for Drilling and Well Servicing Structures. American Petroleum Institute.

Arabian Drilling Company. (2018). arabdrill.com, last visited on May 2018.

ASCE/SEI 7-05. (2006). Minimum design loads for buildings and other structures. American Society of Civil Engineers.

ASD-AISC. (1989). Specification for Structural Steel Buildings. American Institute of Steel Construction.

Belegundu, A. D., & Arora, J. S. (1985). A study of mathematical programming

methods for structural optimization. Part I: Theory. International Journal for Numerical Methods in Engineering, 21(9), 1583–1599.

Dorigo, M., & Stützle, T. (2004). Ant Colony Optimization.

Drilling Contractor. (2018). drillingcontractor.org, last visited on May 2018.

Erbatur, F., & Al-Hussainy, M. M. (1992). Optimum design of frames. Computers & Structures, 45(5–6), 887–891.

Erol, O. K., & Eksin, I. (2006). A new optimization method: Big Bang-Big Crunch. Advances in Engineering Software, 37(2), 106–111.

GlobalSpec. (2018). globalspec.com, last visited on May 2018.

Hager, K., & Balling, R. (1988). New Approach for Discrete Structural Optimization. Journal of Structural Engineering, 114(5), 1120–1134.

Hasançebi, O., & Azad, S. K. (2014). Discrete size optimization of steel trusses using a refined big bang–big crunch algorithm. Engineering Optimization, 46(1), 61–83.

Hasançebi, O., & Azad, S. K. (2015). Adaptive dimensional search: A new metaheuristic algorithm for discrete truss sizing optimization. Computers and Structures, 154, 1–16.

Hasançebi, O., Bahçecioğlu, T., Kurç, Ö., & Saka, M. P. (2011). Optimum design of high-rise steel buildings using an evolution strategy integrated parallel algorithm. Computers & Structures, 89(21–22), 2037–2051.

Hasançebi, O., & Kazemzadeh Azad, S. (2012). An exponential big bang-big crunch algorithm for discrete design optimization of steel frames. Computers & Structures, 110–111, 167–179.

108

Holland, J. H. (John H. (1992). Adaptation in natural and artificial systems : an introductory analysis with applications to biology, control, and artificial intelligence. MIT Press.

ISO 19901-2. (2017). Petroleum and natural gas industries -- Specific requirements for offshore structures -- Part 2: Seismic design procedures and criteria. International Organization for Standardization.

Jorge h.b. Sampayo. (2007). Drilling Engineering Fundamentals.

Kameshki, E. S., & Saka, M. P. (2001). Genetic algorithm based optimum bracing design of non-swaying tall plane frames. Journal of Constructional Steel Research, 57(10), 1081–1097.

Karaboga, D., & Basturk, B. (2007). A powerful and efficient algorithm for numerical function optimization: Artificial bee colony (ABC) algorithm. Journal of Global Optimization, 39(3), 459–471.

Kaveh, A., & Ilchi Ghazaan, M. (2016). A hybrid ECBO and UBS algorithm for optimal design of skeletal structures, 17(7), 917–936.

Kaveh, A., & Talatahari, S. (2009a). Particle swarm optimizer, ant colony strategy and harmony search scheme hybridized for optimization of truss structures. Computers and Structures, 87(5–6), 267–283.

Kaveh, A., & Talatahari, S. (2009b). Size optimization of space trusses using Big Bang–Big Crunch algorithm. Computers & Structures, 87(17–18), 1129–1140.

Kaveh, A., & Talatahari, S. (2010). Optimal design of Schwedler and ribbed domes via hybrid Big Bang–Big Crunch algorithm. Journal of Constructional Steel

Research, 66(3), 412–419.

Kazemzadeh Azad, S. (2017). Enhanced hybrid metaheuristic algorithms for optimal sizing of steel truss structures with numerous discrete variables. Structural and Multidisciplinary Optimization, 55(6), 2159–2180.

Kazemzadeh Azad, S., & Hasançebi, O. (2015). Computationally efficient discrete sizing of steel frames via guided stochastic search heuristic. Computers & Structures, 156, 12–28.

Kazemzadeh Azad, S., Hasançebi, O., & Kazemzadeh Azad, S. (2013). Upper bound strategy for metaheuristic based design optimization of steel frames. Advances in Engineering Software, 57, 19–32.

Kazemzadeh Azad, S., Hasançebi, O., & Saka, M. P. (2014). Guided stochastic search technique for discrete sizing optimization of steel trusses: A design-driven heuristic approach. Computers & Structures, 134, 62–74.

Kennedy, J., & Eberhart, R. (1995). Particle swarm optimization. Neural Networks, 1995. Proceedings., IEEE International Conference On, 4, 1942–1948 vol.4.

Kennedy, J. F., Eberhart, R. C., & Shi, Y. (2001). Swarm intelligence. Morgan Kaufmann Publishers.

Khatibinia, M., & Yazdani, H. (2018). Accelerated multi-gravitational search algorithm for size optimization of truss structures. Swarm and Evolutionary Computation, 38, 109–119.

Lee C. Moore. (2018). lcm-wci.com, last visited on May 2018.

Lee, K. S., & Geem, Z. W. (2004). A new structural optimization method based on the harmony search algorithm. Computers and Structures, 82(9–10), 781–798.

Loadmaster Universal Rigs Inc. (2018). loadmasterur.com, last visited on May 2018.

LRFD-AISC. (1994). Manual of steel construction-Load and Resistance Factor Design. American Institute of Steel Construction.

LRFD-AISC. (2016). Specification for Structural Steel Buildings. American Institute of Steel Construction.

National Driller Magazine. (2018). nationaldriller.com, last visited on May 2018.

Nickabadi, A., Ebadzadeh, M. M., & Safabakhsh, R. (2011). A novel particle swarm optimization algorithm with adaptive inertia weight. Applied Soft Computing, 11(4), 3658–3670.

Prayogo, D., Cheng, M.-Y., Wu, Y.-W., Herdany, A. A., & Prayogo, H. (2018). Differential Big Bang - Big Crunch algorithm for construction-engineering design optimization. Automation in Construction, 85, 290–304.

Rigzone Inc. (2018). rigzone.com, last visited on May 2018.

Saka, M. P. (1991). Optimum design of steel frames with stability constraints. Computers & Structures, 41(6), 1365–1377.

SAP2000 v19.2.2. (2017). Computers and Structures Inc. Berkeley, CA.

Sunnda Corporation. (2018). sunnda.com, last visited on May 2018.

Tang, H., Zhou, J., Xue, S., & Xie, L. (2010). Big Bang-Big Crunch optimization for parameter estimation in structural systems.

Tejani, G. G., Savsani, V. J., Patel, V. K., & Savsani, P. V. (2018). Size, shape, and topology optimization of planar and space trusses using mutation-based improved metaheuristics. Journal of Computational Design and Engineering,

5(2), 198–214.

Turner, J. W., Company, E. D., Effenberger, M., Services, S. E., & Irick, J. (2002). IADC / SPE 74454 Seismic Assessment Procedures for Drilling Structures on Offshore Platforms.

Venkayya, V. B. (1978). Structural optimization: A review and some recommendations. International Journal for Numerical Methods in Engineering, 13(2), 203–228.

Yang, X.-S. (2010). Nature-inspired metaheuristic algorithms. Luniver Press.

Yang, X. S. (2013). Metaheuristic optimization: Nature-inspired algorithms and applications. Studies in Computational Intelligence.

Yuhui Shi, & Eberhart, R. C. (2001). Fuzzy adaptive particle swarm optimization. In Proceedings of the 2001 Congress on Evolutionary Computation (IEEE Cat. No.01TH8546) (Vol. 1, pp. 101–106). IEEE.